

The Choice of Line Lengths in Multiline Thru-Reflect-Line Calibration

Ziad Hatab, Michael E. Gadringer, and Wolfgang Bösch
 Graz University of Technology, Austria
 michael.gadringer@tugraz.at

Abstract—This paper presents an analysis and rigorous procedure for determining the optimal lengths of line standards in multiline thru-reflect-line (TRL) calibration of vector network analyzers (VNAs). The solution is obtained through nonlinear constrained optimization of the eigenvalue problem in multiline TRL calibration. Additionally, we propose a simplified approach for near-optimal length selection based on predefined sparse rulers. Alongside the length calculation, we discuss the required number of lines to meet bandwidth requirements. The sensitivity of the proposed procedure is evaluated numerically via Monte Carlo simulations, demonstrating that the derived lengths have lower uncertainty than those from existing industry standards. Practical examples are provided for various applications, including lossy and dispersive lines, as well as banded solutions for waveguides.

Index Terms—vector network analyzer, calibration, metrology, microwave measurement

I. INTRODUCTION

M EASUREMENT traceability for scattering parameters (S-parameters) at microwave frequencies is established through calibration procedures. An important vector network analyzer (VNA) calibration technique is the thru-reflect-line (TRL) method [1]. This calibration approach leverages the characteristic impedance of the line and thru standard to determine the calibration's reference impedance. For metrology applications, air lines are used for this purpose [2]. Due to their simple mechanical setup, air lines allow linking the lines' characteristic impedance to their material properties (permittivity, permeability, conductivity) and geometrical dimensions, as the isolating material (air) is well known and the geometrical dimensions can be measured traceably to the SI system of units. The same approach can be applied to lines manufactured with different materials and manufacturing technologies, which explains the widespread use of TRL calibration. For broadband measurements, the multiline TRL [3], [4] was suggested, which employs multiple transmission lines with identical cross-sectional properties but different lengths.

The classical TRL formulation involves a single eigenvalue problem based on the length difference between the thru and line standards. Selecting this length difference is straightforward, as the eigenvalue problem exhibits optimal stability when the eigenvalue phases are $\pm 90^\circ$. The eigenvalues, being

This work was supported by the Christian Doppler Research Association, the Austrian Federal Ministry for Digital and Economic Affairs, and the National Foundation for Research, Technology and Development.

<https://github.com/ziadhatab/line-length-multiline-trl-calibration>

phase conjugates, coincide at phases $\pm 0^\circ$ or $\pm 180^\circ$. The $\pm 90^\circ$ phase occurs at a single frequency, typically chosen as the center frequency. The usable bandwidth is then defined by arbitrary phase margins as thresholds, commonly between $\pm 20^\circ$ and $\pm 30^\circ$ [5]. Due to the cyclic nature of the phase, TRL can cover multiple bands, with the fundamental band at quarter-wavelengths. This property enables the use of longer line lengths for waveguides, resulting in “3/4-wave” or “5/4-wave” TRL kits [6]–[8].

While length selection in lossless TRL calibration is straightforward, losses introduce complications. With losses, eigenvalues follow a spiral rotation in the complex plane and never exactly coincide at phases $\pm 0^\circ$ or $\pm 180^\circ$. Higher losses cause the line to more closely resemble a load standard, thereby broadening its bandwidth. This broadening assumes that the thru standard's back-to-back length is not so long as to introduce significant losses, which would impede transmission. The line standard, however, can be very lossy, and in extreme cases can be replaced by a load, resulting in thru-reflect-match (TRM) calibration [9].

As modern radio frequency (RF) and millimeter-wave (mmWave) applications demand wider bandwidth measurements, multiline TRL calibration has become essential. Despite the existence of multiline TRL algorithms for over three decades [3], [4], [10], [11], optimal line length selection remains understudied. Current literature primarily focuses on selecting line lengths relative to the thru standard based on phase margin transitions. The Microwaves101 online resource provides a useful spreadsheet [5] that determines appropriate lengths based on relative effective permittivity. Similar approaches are discussed in [3], [6], [12]–[15]. It is important to note that these methods apply to the lossless multiline TRL case. Including the losses in this evaluation can relax the phase-margin constraints.

A fundamental challenge in optimizing line length selection arises from the multiline TRL implementation method itself. Traditional approaches decompose the problem into several TRL pairs with a common reference line [3], [10]. Since these methods independently select reference lines at each frequency point, they complicate the problem formulation, leading to the current conventional approach of fixing the thru as the reference when computing the lengths.

This article rigorously formulates the line length selection problem based on the multiline procedure in [4]. This method reduces the multiline problem to solving a single weighted eigenvalue problem, enabling a formulation similar to the

classical TRL calibration.

The remainder of this article is organized as follows: Section II analyzes the frequency limitations in classical TRL and multiline TRL methods, introducing the concept of effective phase for multiline TRL calibration. Section III develops an optimization approach for line length selection based on minimizing eigenvector sensitivity and introduces a simplified line selection method using sparse rulers, as well as a discussion on determining the recommended number of lines for a given frequency bandwidth. Section IV presents numerical sensitivity analysis, while Section V provides examples of computing line lengths for different scenarios. Lastly, Section VI offers concluding remarks.

II. FREQUENCY LIMITATION IN TRL AND MULTILINE TRL CALIBRATIONS

The purpose of this section is to review the frequency limitations in both classical TRL and multiline TRL methods, and to explain the relationship between line length and frequency based on the eigenvalues. Additionally, we introduce the concept of an effective phase for multiline TRL calibration, which aims to provide a phase concept similar to that used in the classical TRL method. The development of this measure will allow us to compare the performance of line length sets even with different numbers of lines.

In both classical TRL and multiline TRL, we use the error box model that describes a two-port VNA, as shown in Fig. 1. This model applies the matrix product for T-parameters to establish the desired relationship:

$$\mathbf{M}_i = k_a k_b \underbrace{\begin{bmatrix} a_{11} & a_{12} \\ a_{21} & 1 \end{bmatrix}}_A \underbrace{\begin{bmatrix} e^{-\gamma l_i} & 0 \\ 0 & e^{\gamma l_i} \end{bmatrix}}_{L_i} \underbrace{\begin{bmatrix} b_{11} & b_{12} \\ b_{21} & 1 \end{bmatrix}}_B \quad (1)$$

where \mathbf{A} and \mathbf{B} are the left and right error boxes and k is the transmission error term. The matrix \mathbf{L}_i corresponds to the line model of the i th measured line.

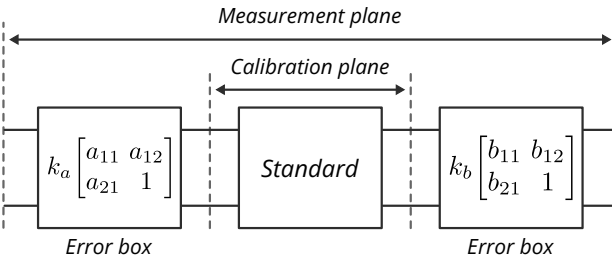


Fig. 1. Error box model of a two-port VNA for the measurement of calibration standards.

A. Eigenvalues in Classical TRL

For the discussion that follows, we maintain generality by using a non-zero length line instead of a thru standard, known as line-reflect-line (LRL) calibration [16]. When considering two lines of different lengths, we can formulate an eigenvalue problem by taking the T-parameters measurements of two lines and multiplying the inverse of one by the other:

$$\mathbf{M}_i \mathbf{M}_j^{-1} = \mathbf{A} \begin{bmatrix} e^{-\gamma l_{ij}} & 0 \\ 0 & e^{\gamma l_{ij}} \end{bmatrix} \mathbf{A}^{-1}, \quad l_{ij} = l_i - l_j. \quad (2)$$

The eigenvalues depend on the complex propagation constant γ , which is frequency-dependent and can be expressed in terms of the relative effective permittivity [17] as follows:

$$\gamma = \alpha + j\beta = \frac{2\pi f}{c_0} \sqrt{-\epsilon_{r,\text{eff}}} \quad (3)$$

where $\epsilon_{r,\text{eff}} = \epsilon'_{r,\text{eff}} - j\epsilon''_{r,\text{eff}}$, f is the frequency, and c_0 is the speed of light in vacuum. In (3), while the frequency dependence of the propagation constant is linear with respect to $\epsilon_{r,\text{eff}}$, in general $\epsilon_{r,\text{eff}}$ itself can be frequency-dependent. Thus the propagation constant can be nonlinear with frequency. The special case where $\epsilon_{r,\text{eff}}$ remains constant occurs only in transmission lines that support a single transverse electromagnetic mode (TEM) [18].

The real part of γ represents attenuation per unit length, while the imaginary part relates to the wave's velocity. As γ varies with frequency, the eigenvalues rotate in the complex plane, as illustrated in Fig. 2a for both lossless and lossy cases.

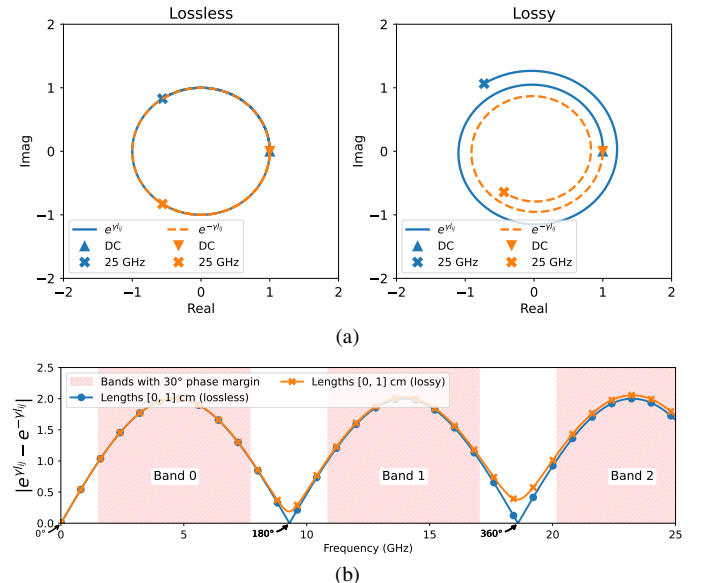


Fig. 2. Example illustrating the evolution of the eigenvalues in classical TRL calibration as a function of frequency. (a) Complex plane representation, (b) the eigengap response. Parameters used in this example: length difference of 1 cm, frequency range of 0-25 GHz, and $\epsilon_{r,\text{eff}} = 2.6$ for the lossless case, while $\epsilon_{r,\text{eff}} = 2.6(1 - 0.06j)$ for the lossy case.

In classical TRL, frequency limitations are most pronounced in lossless transmission lines. The eigenvalues become identical when the phase γl_{ij} equals 0° or 180° (or their integer multiples). At these critical points, the eigendecomposition fails, making it impossible to extract the error box parameters. This limitation is most severe in the ideal lossless case, where the propagation constant simplifies to $\gamma_{\text{lossless}} = j\beta = \frac{2\pi f}{c_0} j \sqrt{\epsilon'_{r,\text{eff}}}$. Fig. 2b demonstrates this phenomenon by showing how the eigengap (the error vector magnitude between eigenvalues) reaches zero at these points.

To ensure reliable calibration, the line length difference should maintain eigenvalues within a phase margin, avoiding

the 0° and 180° points. The calibration boundaries, incorporating a phase margin, are:

$$\pi n + \pi \frac{\varphi}{180} \leq l_{ij} \frac{2\pi f}{c_0} \sqrt{\epsilon'_{r,eff}} \leq \pi n + \left(1 - \frac{\varphi}{180}\right) \pi \quad (4)$$

where φ is the phase margin in degrees and $n = 0, 1, 2, \dots$ indicates the band number, with $n = 0$ being the fundamental band (e.g., see Fig. 2b). This can be rewritten as frequency bounds as follows:

$$\frac{n + \varphi/180}{2l_{ij}\sqrt{\epsilon'_{r,eff}}} c_0 \leq f \leq \frac{n + 1 - \varphi/180}{2l_{ij}\sqrt{\epsilon'_{r,eff}}} c_0, \quad (5)$$

or as minimum and maximum frequencies as follows:

$$f_{\min} = \frac{n + \varphi/180}{2l_{ij}\sqrt{\epsilon'_{r,eff}}} c_0, \quad f_{\max} = \frac{n + 1 - \varphi/180}{2l_{ij}\sqrt{\epsilon'_{r,eff}}} c_0. \quad (6)$$

The required line length difference can be determined by solving either of the equations in (6), leading to:

$$l_{ij} = \frac{c_0}{2f_{\min}\sqrt{\epsilon'_{r,eff}}} \left(n + \frac{\varphi}{180}\right), \quad (7a)$$

$$l_{ij} = \frac{c_0}{2f_{\max}\sqrt{\epsilon'_{r,eff}}} \left(n + 1 - \frac{\varphi}{180}\right), \quad (7b)$$

For (7) to be consistent for given minimum and maximum frequencies, the phase wrapping constant n can be determined by equating both equations, which yields:

$$n = \left\lfloor \frac{q - (q + 1)\varphi/180}{1 - q} \right\rfloor, \quad (8)$$

where $q = f_{\min}/f_{\max}$.

Since n must be an integer, the actual achieved phase margin for given frequency requirements becomes:

$$\varphi = 180 \frac{nq - n + q}{q + 1}. \quad (9)$$

For wide bandwidth requirements, the calculation from (8) will result in $n < 1$, which forces $n = 0$. Consequently, the achieved phase margin may be less than specified. For phase margins $\geq 20^\circ$, it is recommended that $f_{\max} \leq 8f_{\min}$. Generally, for phase margins between 0° and 90° at the fundamental band (i.e., $n = 0$), the relationship between minimum and maximum frequencies must satisfy:

$$f_{\max} \leq \frac{180 - \varphi}{\varphi} f_{\min}. \quad (10)$$

Once n is determined for a given phase margin and frequency limits, the line length difference l_{ij} can be calculated using either (7a) or (7b). Note that throughout (4)-(10), $\epsilon'_{r,eff}$ is treated as constant. While this is generally not true, we can use either an $\epsilon'_{r,eff}$ averaged over the covered frequency range or the DC value for quasi-TEM transmission lines.

B. Eigenvalues in Multiline TRL

This section discusses the multiline TRL formulation from [4]. This approach differs from traditional multiline TRL calibration implementations by using a Kronecker product formulation, where the error box model of each line is vectorized using Kronecker product properties, as written below:

$$\text{vec}(\mathbf{M}_i) = k(\mathbf{B}^T \otimes \mathbf{A})\text{vec}(\mathbf{L}_i), \quad (11)$$

where \otimes is the Kronecker product and $\text{vec}(\cdot)$ is the vectorization operation [19]. The terms \mathbf{A} , \mathbf{B} , k , and \mathbf{L}_i are the same as given in (1).

For $N \geq 2$ lines, the equations describing the error boxes for all line measurements are summarized in two equations as given below:

$$\mathbf{M} = k\mathbf{X}\mathbf{L}, \quad (12a)$$

$$\mathbf{D}^{-1}\mathbf{M}^T\mathbf{P}\mathbf{Q} = \frac{1}{k}\mathbf{L}^T\mathbf{P}\mathbf{Q}\mathbf{X}^{-1}, \quad (12b)$$

where

$$\mathbf{M} = [\text{vec}(\mathbf{M}_1) \quad \text{vec}(\mathbf{M}_2) \quad \cdots \quad \text{vec}(\mathbf{M}_N)], \quad (13a)$$

$$\mathbf{L} = [\text{vec}(\mathbf{L}_1) \quad \text{vec}(\mathbf{L}_2) \quad \cdots \quad \text{vec}(\mathbf{L}_N)], \quad (13b)$$

$$\mathbf{X} = \mathbf{B}^T \otimes \mathbf{A}, \quad (13c)$$

$$\mathbf{D} = \text{diag}([\det(\mathbf{M}_1) \quad \cdots \quad \det(\mathbf{M}_N)]), \quad (13d)$$

$$\mathbf{P} = \begin{bmatrix} 1 & 0 & 0 & 0 \\ 0 & 0 & 1 & 0 \\ 0 & 1 & 0 & 0 \\ 0 & 0 & 0 & 1 \end{bmatrix}, \quad \mathbf{Q} = \begin{bmatrix} 0 & 0 & 0 & 1 \\ 0 & -1 & 0 & 0 \\ 0 & 0 & -1 & 0 \\ 1 & 0 & 0 & 0 \end{bmatrix}. \quad (13e)$$

The eigenvalue problem is formulated by first multiplying an $N \times N$ weighting matrix \mathbf{W} on the right-hand side of (12a), and then multiplying this result on the left-hand side of (12b), resulting in:

$$\underbrace{\mathbf{M}\mathbf{W}\mathbf{D}^{-1}\mathbf{M}^T\mathbf{P}\mathbf{Q}}_{\mathbf{F}: 4 \times 4} = \mathbf{X} \underbrace{\mathbf{L}\mathbf{W}\mathbf{L}^T\mathbf{P}\mathbf{Q}}_{\mathbf{H}: 4 \times 4} \mathbf{X}^{-1}. \quad (14)$$

The equation in (14) represents a similarity transformation between matrices \mathbf{F} and \mathbf{H} , with \mathbf{X} as the transformation matrix. By choosing an appropriate \mathbf{W} as described in [4], matrix \mathbf{H} becomes diagonal, transforming the similarity problem into an eigenvalue problem:

$$\mathbf{F} = \mathbf{X} \begin{bmatrix} -\lambda & 0 & 0 & 0 \\ 0 & 0 & 0 & 0 \\ 0 & 0 & 0 & 0 \\ 0 & 0 & 0 & \lambda \end{bmatrix} \mathbf{X}^{-1}, \quad (15)$$

where

$$\lambda = \sum_{\substack{i=1 \\ i < j \leq N}}^{N-1} |e^{\gamma l_{ij}} - e^{-\gamma l_{ij}}|^2 = \frac{1}{2} \|\mathbf{W}\|_F^2. \quad (16)$$

The details on computing \mathbf{W} are found in [4] and [20]. The solution for the calibration coefficients is obtained from the eigenvectors associated with eigenvalues $\pm\lambda$. A solution exists only when λ is non-zero. Similar to classical TRL, if

we consider only two lines, λ becomes zero at $\gamma l_{ij} = 0^\circ$ and $\gamma l_{ij} = 180^\circ$ (or their integer multiples).

Unlike classical TRL, deriving analytical expressions for optimal line lengths is not possible for more than two lines due to the multiple terms in the summation of (16). In Section III, we present our proposed methods for computing line lengths via a constrained optimization approach and sparse rulers.

Another important consideration is that the eigenvalue in multiline TRL calibration increases significantly with the number of transmission lines used, which is a natural consequence of multiple line pairs, unlike classical TRL, which uses only a single line pair. Fig. 3 illustrates this eigenvalue behavior for configurations with three and four lines. Specifically, at approximately 5 GHz, the three-line configuration exhibits an eigenvalue of approximately 8, whereas the four-line configuration shows an eigenvalue of approximately 12. Consequently, normalization becomes necessary to enable meaningful comparisons between line sets of different counts and lengths. This normalization approach is discussed in detail in Section II-C.

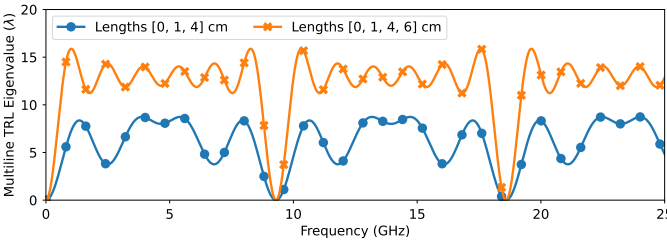


Fig. 3. Example illustrating the eigenvalue behavior in multiline TRL calibration for three and four-line configurations. The figure demonstrates how eigenvalues increase with the number of lines used. Relative effective permittivity assumed lossless $\epsilon_{r,\text{eff}} = 2.6 - 0j$.

It is worth noting that even when using multiple lines to expand the calibration frequency range, the eigenvalue in multiline TRL calibration still exhibits a cyclic behavior in the lossless case. This occurs particularly when the lengths of lines are harmonically related, as depicted in Fig. 3. This periodic behavior is analogous to that observed in classical TRL, enabling multiple usable frequency bands across the spectrum. For lossy lines, the eigenvalue λ never reaches zero except at DC frequency.

C. Defining an Effective Phase for Multiline TRL

We now define an effective phase for multiline TRL. Unlike classical TRL, associating the phase with the multiline TRL is challenging due to the multiple line pairs summed in the eigenvalue expression of (16). Furthermore, since the eigenvalue in multiline TRL increases with the number of lines, direct comparison with classical TRL or quantifying which set of lines performs better becomes difficult. Therefore, we need a normalization that scales properly with the number of lines.

Introducing such normalization to the multiline TRL eigenvalue does not affect the weighted eigendecomposition in (14), as all eigenvalues are scaled by the same factor. The sensitivity of the eigenvectors remains unaffected as long as this normalization is non-zero. Using this normalized eigenvalue, we can define an effective phase equivalent to that of classical TRL.

It is important to note that the phase concept in TRL is just one established metric for classical TRL that we use for historical consistency. Additionally, when two sets of line lengths yield the same phase response but one set uses more lines, the set with more lines naturally performs better in the presence of measurement noise and perturbations. This improved performance results from having more measurements. Additionally, the eigenvector sensitivity is inversely proportional to the eigengap [21]. This is further discussed in Section III-A.

As established so far, the stability of multiline TRL relies on the eigenvalue in (16) being non-zero for all considered frequencies. While the multiline TRL formulation appears more complicated than classical TRL, it actually reduces to classical TRL in the special case of two lines. In fact, the eigenvalue λ becomes the square of the eigengap used to define the phase in TRL; that is, taking the square root of the multiline TRL eigenvalue for two lines is equivalent to the eigengap in classical TRL:

$$|e^{\gamma l_{12}} - e^{-\gamma l_{12}}| = \sqrt{\lambda_{\text{TRL}}}, \quad l_{12} = l_1 - l_2. \quad (17)$$

From the above equation, it is clear that the phase of a classical TRL can be defined from the eigenvalue λ as follows:

$$\phi = \arcsin\left(\frac{\sqrt{\lambda_{\text{TRL}}}}{2}\right), \quad (18)$$

where for the lossless case, (18) is confined between 0° and 90° . For the lossy case, any value exceeding the limits of the arcsine function by convention is truncated to 90° [3].

For two lines, as in (17) and (18), it is straightforward to define a phase, since there is only one line pair. However, when more than two lines are used, the eigenvalue increases, even in the lossless case, simply because there are more line pairs. However, this does not necessarily mean that the bandwidth of the multiline TRL is improved. As highlighted earlier, this means that the sensitivity of the eigenvectors improves against noise and perturbations in the measurements. For example, suppose we have three lines, where two are identical, i.e., $\mathbf{l} = \{l_1, l_2, l_2\}$. This is no different from classical TRL, but now there are three pairs, one of which has zero length difference:

$$\lambda = |e^{\gamma l_{12}} - e^{-\gamma l_{12}}|^2 + |e^{\gamma l_{13}} - e^{-\gamma l_{13}}|^2 + \underbrace{|e^{\gamma l_{23}} - e^{-\gamma l_{23}}|^2}_{=0} \quad (19)$$

To define a phase for this example, which should match the classical TRL case in (17), we solve for the eigengap as follows:

$$|e^{\gamma l_{12}} - e^{-\gamma l_{12}}| = \sqrt{\lambda/2}, \quad \text{or} \quad \phi = \arcsin\left(\frac{\sqrt{\lambda/2}}{2}\right) \quad (20)$$

In general, for multiple lines of different lengths, the eigenvalue summation in (16) involves all line pairs, not just one as in the repeated line example. To accommodate the general case, we need an average metric for all line pairs. A natural choice is the root mean square (RMS), since the eigenvalue sums over squared terms, and we need to take the square root to use it in the arcsin function to measure phase. To obtain the

average, we scale by the number of line pairs before taking the square root:

$$\phi = \arcsin \left(\frac{\sqrt{\lambda/C(N, 2)}}{2} \right) \quad (21)$$

where $C(N, 2) = N(N - 1)/2$ is the number of unique line pairs.

While (21) meets our needs in many cases, it does not adequately handle repeated line pairs. For example, in the previous example of three lines with one line repeated, the denominator under the square root should be 2, but (21) would give 3, which is incorrect. Clearly, we need to modify the scaling to account for repeated lines and for line pairs with a very small eigengap.

This motivates a normalization that also depends on the line lengths. We start by rewriting the eigenvalue expression in (16) as a weighted sum:

$$\lambda = \sum_{\substack{i=1 \\ i < j \leq N}}^{N-1} |e^{\gamma l_{ij}} - e^{-\gamma l_{ij}}|^2 = \sum_{\substack{i=1 \\ i < j \leq N}}^{N-1} |w_{ij}| \cdot |w_{ij}| \quad (22)$$

where $|w_{ij}| = |e^{\gamma l_{ij}} - e^{-\gamma l_{ij}}|$ is the eigengap of each line pair. Since we are interested in an average metric for $|w_{ij}|$, we should divide the sum by the sum of the $|w_{ij}|$ terms. Thus, a normalized eigenvalue can be written as follows:

$$\kappa = \frac{\lambda}{\sum_{\substack{i=1 \\ i < j \leq N}}^{N-1} |w_{ij}|} = \frac{\lambda}{\|\text{vec}(\mathbf{W})\|_1 / 2} = \frac{\|\text{vec}(\mathbf{W})\|_2^2}{\|\text{vec}(\mathbf{W})\|_1} \quad (23)$$

where $\|\text{vec}(\mathbf{W})\|_2^2 = \|\mathbf{W}\|_{\text{F}}^2$ is the squared L2-norm (Frobenius norm) of the vectorized \mathbf{W} , and $\|\text{vec}(\mathbf{W})\|_1$ is the L1-norm (sum-norm or Manhattan norm) [22].

This new definition of normalized eigenvalue in (23) addresses most of our requirements. For two lines, it reduces to the eigengap of classical TRL:

$$\kappa(l_1, l_2) = |e^{\gamma l_{12}} - e^{-\gamma l_{12}}| \quad (24)$$

For the repeated line example in (19), this normalization also reduces to the classical TRL case:

$$\kappa(l_1, l_2, l_2) = \kappa(l_1, l_2) = |e^{\gamma l_{12}} - e^{-\gamma l_{12}}| \quad (25)$$

However, in general, this normalization does not make the eigenvalue invariant to repeated lines when there are more than two different lines, e.g.,

$$\kappa(l_1, l_2, l_3, l_3) \neq \kappa(l_1, l_2, l_3) \quad (26)$$

While this may seem like a limitation, it is actually not, as the normalization in (23) provides a good average metric for the eigengap, being bounded by the minimum and maximum eigengap of all line pairs due to this self-weighting [23]. Hence, κ is bounded as follows:

$$|w_{ij}|_{\min} \leq \kappa \leq |w_{ij}|_{\max}, \quad \forall i, j \leq N \quad (27)$$

Therefore, κ is always bounded by the best line pair at any frequency point. In fact, due to self-weighting, it is naturally

biased towards the better line pairs. The worst case is when there are line pairs with zero length difference, $|w_{ij}|_{\min} = 0$, and at best for the lossless case, $|w_{ij}|_{\max} = 2$ at quarter-wavelength. Fig. 4 illustrates this normalized eigenvalue using the same example from Fig. 3 for both three and four lines, where the normalized eigenvalue is plotted as a function of frequency.

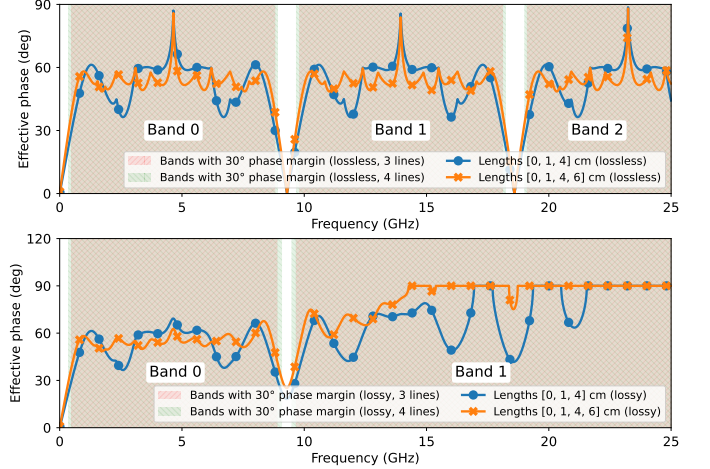


Fig. 4. Comparison of effective phase for three and four lines configurations under both lossless $\epsilon_{r,\text{eff}} = 2.6 - 0j$ and lossy $\epsilon_{r,\text{eff}} = 2.6(1 - 0.06j)$ conditions across the 0-25 GHz frequency range.

To compute an effective phase, we simply use the arcsine function as in (18), and substituting κ in it:

$$\phi = \arcsin \left(\frac{\kappa}{2} \right) \quad (28)$$

A bandwidth can be defined, as in classical TRL, by requiring a phase margin $\phi > \varphi$. The example in Fig. 4 shows the $\varphi = 30^\circ$ phase margin bands for the lossless case for both the three- and four-line examples, which is equivalent to $\kappa \geq 1$.

While the normalized eigenvalue κ is not strictly invariant to repeated lines, it remains a robust metric for comparing sets of lines, even when repeated lines are present. For example, Fig. 5 shows the normalized eigenvalue for multiline TRL calibration using four lines $\{0, 1, 4, 6\}$ cm and six lines $\{0, 1, 4, 6, 6, 6\}$ cm. The only difference is that the last line in the six-line example is repeated, i.e., $l_6 = l_5 = 6$ cm. The figure demonstrates that the normalized eigenvalue for both sets is very similar. The only way to mitigate the effect of repeated lines is to provide that information as part of the weighted eigendecomposition by modifying the weighting matrix, for example, using the scaled version described in Appendix A.

It should be noted that, due to averaging, the maximum phase of 90° seen in classical TRL is not achieved here. This would require all line pairs to simultaneously have a phase of 90° , which can only occur at discrete frequencies. This does not imply reduced performance; rather, it reflects how all line pairs contribute, each scaled by their own weights, and how measurement noise tends to average out when all lines contribute.

Alternatively, the weighting in multiline TRL could be modified to bias the result toward the line pairs with the higher

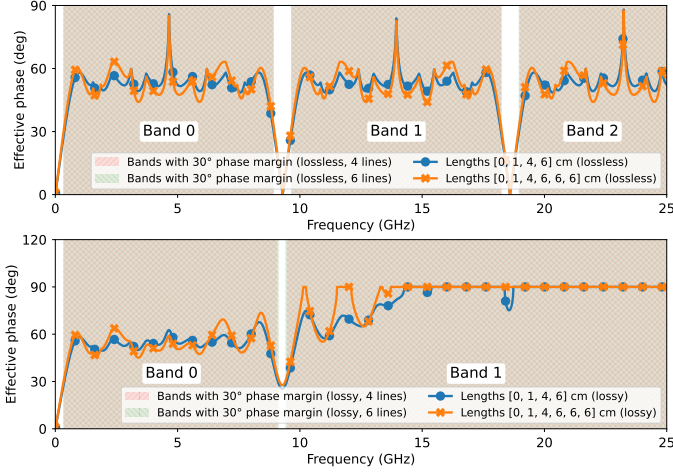


Fig. 5. Comparison of effective phase between four and six-line configurations, where in the six-line configuration, the fourth line is repeated three times. Results are shown for both lossless $\epsilon_{r,\text{eff}} = 2.6 - 0j$ and lossy $\epsilon_{r,\text{eff}} = 2.6(1 - 0.06j)$ conditions across the 0-25 GHz frequency range.

phase by incorporating a scaling matrix into the weighting matrix, as described in Appendix A. This approach would progressively discard line pairs with low phase contribution as the scaling increases, resulting in an outcome that is more biased toward line pairs with higher phase.

The default weighting choice, as in [4], [20], is the L1-norm, where each line pair is weighted by its own eigengap. Increasing the exponent on the eigengap leads to Lm -norm weighting of the line pairs, as discussed in Appendix A. In the extreme case, as the norm approaches ∞ , the weighting acts as $L\infty$ -norm, effectively becoming selective TRL, where at each frequency the line pair with maximum phase is chosen.

III. PROCEDURES FOR COMPUTING LINE LENGTHS FOR MULTILINE TRL CALIBRATION

In this section, we cover three topics. In a first step, we present the brute-force approach for finding optimal line lengths through nonlinear constrained optimization. The second method is a simpler approach using sparse rulers, which, while not optimal, provides a convenient way to quickly compute line lengths. The last topic addresses determining the required number of lines for a given frequency range.

A. The Brute-Force Optimization Method

As elaborated in Subsections II-B and II-C, multiline TRL calibration will only have a solution for the error terms if the eigenvalue λ is non-zero across all considered frequencies. When selecting line lengths, our main concern is the sensitivity of the eigenvectors, as they contain the error terms we are solving for. According to eigenvector perturbation theory [21], the Jacobian of the eigenvectors is inversely proportional to the eigenvalue difference (i.e., the eigengap). For example, given the matrix system \mathbf{F} from (15) and its left and right eigendecompositions $\mathbf{F} = \mathbf{U}\Lambda\mathbf{U}^{-1}$ and $\mathbf{F}^T = \mathbf{V}\Lambda\mathbf{V}^{-1}$,

respectively, where $\mathbf{V} = \mathbf{U}^{-T}$, the Jacobian of the i th eigenvector is given by [19], [24]:

$$\mathbf{J}_{\mathbf{u}_i} = (\mathbf{F} - \mu_i \mathbf{I})^+ \left(\frac{1}{\mathbf{v}_i^T \mathbf{u}_i} (\mathbf{u}_i^T \otimes \mathbf{u}_i \mathbf{v}_i^T) - (\mathbf{u}_i^T \otimes \mathbf{I}) \right) \mathbf{J}_{\mathbf{F}} \quad (29)$$

where μ_i is the i th eigenvalue, and $\mathbf{J}_{\mathbf{u}_i}$ and $\mathbf{J}_{\mathbf{F}}$ are the Jacobians of the i th eigenvector \mathbf{u}_i and the matrix \mathbf{F} , respectively. The symbol $(\cdot)^+$ denotes the pseudo-inverse and \otimes is the Kronecker product.

The pseudo-inverse in (29) indicates that the eigenvector sensitivity is inversely proportional to the eigengap. As presented in (15), we can factor λ out of the equation, leading to the fact that the corresponding Jacobian of the eigenvector is inversely proportional to only λ , i.e.,

$$\mathbf{J}_{\mathbf{u}} \propto \frac{1}{\lambda} \mathbf{J}_{\mathbf{F}} \quad (30)$$

Therefore, to minimize the sensitivity of the eigenvector solutions, we need to maximize the eigenvalue λ across all considered frequencies. This can be formulated as an optimization problem using the following loss function:

$$l_{\text{opt}} = \underset{\mathbf{l}}{\operatorname{argmin}} \frac{1}{2} \left(\max_{f \in [f_{\min}, f_{\max}]} (-\lambda(\mathbf{l}, f)) - \frac{1}{M} \sum_{f=f_{\min}}^{f_{\max}} \lambda(\mathbf{l}, f) \right) \quad (31)$$

where λ is a function of both frequency and line lengths, with other parameters such as relative permittivity being implicit. f_{\min} and f_{\max} are the frequency bounds over which the optimization is performed, and M is the number of frequency points between f_{\min} and f_{\max} . The negative sign is included to convert the maximization problem into a minimization problem. The loss function in (31) consists of two components: the first is a min-max term that ensures the worst-case frequency point is optimized, while the second is the mean of the eigenvalue, which promotes a flat frequency response. In other words, the line lengths are selected to ensure the eigenvalue is maximized while remaining as uniform as possible across all frequency points.

Without constraints, the optimization formulation in (31) is ill-posed, as any common offset in the line lengths would also be a valid solution. To address this, we need to anchor the first line to be the thru and set it to zero by convention. The second degree of freedom is the maximum length. If unconstrained, the optimization may yield nonphysical line lengths, especially to satisfy the low-frequency requirement. Therefore, both the thru and maximum length must be predefined. The optimization problem can be reformulated as a constrained minimization, where the first and last lines are predefined, i.e., $l_1 = 0$ and $l_N = l_{\max}$, and the remaining lines are optimized:

$$l_{\text{opt}} = \underset{\mathbf{l}}{\operatorname{argmin}} \frac{1}{2} \left(\max_{f \in [f_{\min}, f_{\max}]} (-\lambda(\mathbf{l}, f)) - \frac{1}{M} \sum_{f=f_{\min}}^{f_{\max}} \lambda(\mathbf{l}, f) \right) \quad (32)$$

subject to $\mathbf{a} \leq \mathbf{Cl} \leq \mathbf{b}$

where \mathbf{C} is the constraint matrix encoding the linear constraints on the line lengths to ensure each line is unique, ordered, and always smaller than l_{\max} . Vectors \mathbf{a} and \mathbf{b} are the lower and upper bounds, respectively.

The linear constraint has the following structure:

$$\begin{bmatrix} 0 \\ -l_{\max} \\ -l_{\max} \\ \vdots \\ -l_{\max} \\ l_{\max} \end{bmatrix}_{a:(N+1) \times 1} \leq \underbrace{\begin{bmatrix} -1 & 0 & 0 & \cdots & 0 \\ 1 & -1 & 0 & \cdots & 0 \\ 0 & 1 & -1 & \cdots & 0 \\ \vdots & \vdots & \ddots & \ddots & \vdots \\ 0 & 0 & \cdots & 1 & -1 \\ 0 & 0 & \cdots & 0 & 1 \end{bmatrix}_{C:(N+1) \times N}}_{l:N \times 1} \leq \begin{bmatrix} 0 \\ -l_{\min} \\ -l_{\min} \\ \vdots \\ -l_{\min} \\ l_{\max} \end{bmatrix}_{b:(N+1) \times 1} \quad (33)$$

where l_{\min} and l_{\max} are the minimum and maximum allowed length differences. Note that the first and last entries enforce the first line to be zero length and the last line to have the maximum length. Generally, the choice for l_{\max} is dictated by the minimum required frequency, which can be calculated from (7a), whereas l_{\min} is dictated by the maximum desired frequency, but is also restricted by the minimum resolution of length that can be manufactured.

To select f_{\min} and f_{\max} for the optimization, we use the TRL formulation and choose the frequencies closest to the peaks in the eigengap curve for the longest line length relative to the thru, corresponding to a 90° phase as given by (6). For example, Fig. 6 shows the TRL eigengap curve for $l_{\max} = 6$ cm, where f_{\min} is chosen at the quarter-wavelength of band-0 and f_{\max} at the quarter-wavelength of band-5. We avoid selecting f_{\min} at the desired phase margin (e.g., $\phi = 30^\circ$) because the tail of the multiline TRL eigenvalue will limit the optimization; the lower end cannot be maximized beyond the response of the longest line. The choice of f_{\max} is user-defined, but it affects the minimum possible line length and the required number of lines. In general, a higher f_{\max} requires shorter lines and a greater number of lines.

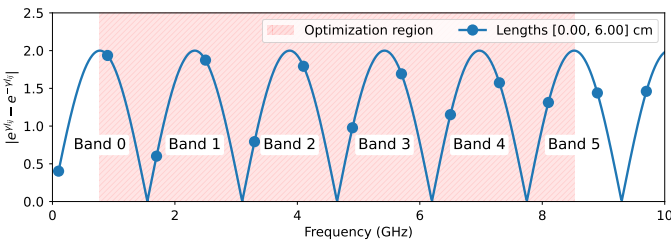


Fig. 6. Illustration of the optimization frequency range determined from the TRL eigengap curve for the longest line. In this example, $l_{\max} = 6$ cm and $\epsilon_{r,\text{eff}} = 2.6 - 0j$, which leads to a minimum frequency anchored at $f_{\min} = 0.775$ GHz (band-0). The maximum frequency was chosen at $f_{\max} = 8.521$ GHz (band-5).

While the minimization formulation in (32) is suitable for obtaining unique, optimal line lengths, this constrained problem can yield solutions that are sensitive to length perturbations, e.g., due to manufacturing and measurement uncertainties. Therefore, it can be beneficial to seek line length solutions that remain near optimal even under known perturbations. To this end, we regularize the objective function in (32) to also

minimize the standard deviation of the eigenvalue:

$$\begin{aligned} l_{\text{opt}} = \underset{l}{\operatorname{argmin}} & \left(\frac{1}{2} \left(\max_{f \in [f_{\min}, f_{\max}]} (-\lambda(l, f)) - \frac{1}{M} \sum_{f=f_{\min}}^{f_{\max}} \lambda(l, f) \right) \right. \\ & \left. + \sqrt{\frac{1}{M} \sum_{f=f_{\min}}^{f_{\max}} \mathbf{J}_{\lambda}(l, f) \Sigma \mathbf{J}_{\lambda}^T(l, f)} \right) \\ \text{subject to } & \mathbf{a} \leq \mathbf{Cl} \leq \mathbf{b} \end{aligned} \quad (34)$$

where $\mathbf{J}_{\lambda}(l, f)$ is the Jacobian of λ with respect to the lengths \mathbf{l} , while Σ is the covariance matrix of the line lengths, which in most cases can be simplified as a scalar, as each line would experience the same perturbation and are often uncorrelated. The details on the calculation of Jacobian $\mathbf{J}_{\lambda}(l, f)$ are provided in Appendix B.

To solve the optimization problem for either (32) or (34), an appropriate optimization procedure is required. Although it may seem that any optimization method would suffice, the loss functions in (32) and (34) are not well-behaved; they exhibit multiple local minima due to the complex exponential terms. As a result, gradient-based optimization methods often fail, becoming trapped in local minima.

To illustrate this concept, consider a system with four lines, where the first and last are anchored at 0 cm and 6 cm, respectively, with $\epsilon_{r,\text{eff}} = 2.6 - 0j$. Fig. 7 displays the loss function landscape when searching for optimal values of l_2 and l_3 using the two loss functions defined in (32) and (34). Due to the symmetry of the search space, we only examine the upper triangular region, which ensures unique line lengths as enforced by the linear constraints. For the regularized loss function in (34), in this example we assumed a length uncertainty of 0.2 cm for each line, resulting in a covariance matrix $\Sigma = (0.2 \text{ cm})^2 \mathbf{I}$.

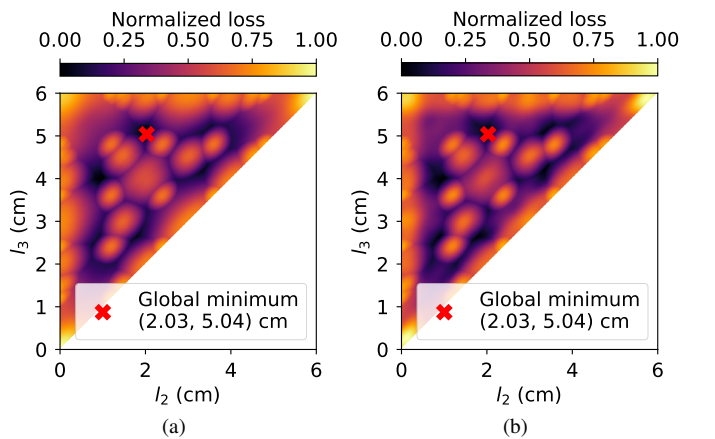


Fig. 7. Grid search visualization for optimizing two line lengths in a four-line system. (a) Loss function landscape using the standard formulation in (32), and (b) loss function with length uncertainty regularization from (34), both computed with $\epsilon_{r,\text{eff}} = 2.6 - 0j$.

As shown in Fig. 7, both loss functions exhibit multiple local minima, making gradient-based optimization challenging. Therefore, we recommend solving such problems using global optimization methods, such as the differential evolution (DE)

algorithm [25]. It is also worth noting that, in Fig. 7, both loss functions yielded the same global minimum. However, this is not necessarily the case in general, especially when considering more complex problems involving multiple lines. Typically, the regularized loss function with length uncertainty produces a more spread distribution of peaks and valleys in the loss function landscape.

Additional regularization or constraints can always be introduced to further restrict the solution space. For example, we may wish to constrain the solution so that the line lengths fit within a predefined physical area. This is particularly relevant for on-wafer applications, where available space is often limited. Typically, the maximum allowable lateral space is assigned to l_{\max} , with the remaining lines arranged in a second row, and so on. Fig. 8 illustrates an example in which four coplanar waveguide (CPW) lines are fitted into two rows: the first row is fully occupied by the longest line, while the second row contains the remaining lines. The objective is to determine the lengths of the other lines such that the total length of each row and the spacing between lines are constant.

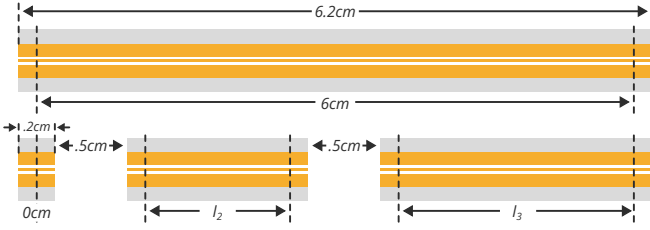


Fig. 8. Illustration of four CPW lines arranged in two rows to optimize space utilization for multiline TRL calibration.

To achieve the constraint shown in Fig. 8, we incorporate an additional linear equality constraint on the lengths, such that the sum of lengths must equal some constraint. The optimization problem is extended from (34) to become:

$$\begin{aligned} \mathbf{l}_{\text{opt}} = \underset{\mathbf{l}}{\operatorname{argmin}} & \left(\frac{1}{2} \left(\max_{f \in [f_{\min}, f_{\max}]} (-\lambda(\mathbf{l}, f)) - \frac{1}{M} \sum_{f=f_{\min}}^{f_{\max}} \lambda(\mathbf{l}, f) \right) \right. \\ & \left. + \sqrt{\frac{1}{M} \sum_{f=f_{\min}}^{f_{\max}} \mathbf{J}_{\lambda}(\mathbf{l}, f) \Sigma \mathbf{J}_{\lambda}^T(\mathbf{l}, f)} \right) \\ \text{subject to } & \mathbf{a}_1 \leq \mathbf{C}_1 \mathbf{l} \leq \mathbf{b}_1 \quad \& \quad \mathbf{C}_2 \mathbf{l} = \mathbf{b}_2 \end{aligned} \quad (35)$$

where $\mathbf{C}_2 \mathbf{l} = \mathbf{b}_2$ is the additional linear constraint. For the example in Fig. 8, the linear constraint matrix \mathbf{C}_2 and equality bound \mathbf{b}_2 will have the following structure:

$$\underbrace{\begin{bmatrix} 0 & 0 & 0 & 1 \\ 1 & 1 & 1 & 0 \end{bmatrix}}_{\mathbf{C}_2} \underbrace{\begin{bmatrix} l_1 \\ l_2 \\ l_3 \\ l_4 \end{bmatrix}}_{\mathbf{l}} = \underbrace{\begin{bmatrix} 6.2 \text{ cm} - 0.2 \text{ cm} \\ 6.2 \text{ cm} - 1 \text{ cm} - 0.6 \text{ cm} \end{bmatrix}}_{\mathbf{b}_2} \quad (36)$$

Each additional linear constraint increases the complexity of the optimization problem by expanding the solution space and introducing more parameters [26]. As a result, such problems may require significantly more time to converge.

We conclude this subsection with a summary of the optimization procedure provided in Algorithm 1.

Algorithm 1 Computing line lengths for multiline TRL calibration based on constrained optimization.

Require: Frequency bounds f_{\min} , f_{\max} , complex relative equivalent permittivity $\epsilon_{r,\text{eff}}$, and the thru length defined to have zero length by convention, i.e., $l_1 = 0$.

- 1: If not provided, compute l_{\max} from f_{\min} and desired minimum phase margin ϕ based on (7a).
- 2: If not provided, determine the number of lines based on the procedure discussed in Subsection III-C.
- 3: Construct constraint matrix \mathbf{C} and bounds \mathbf{a} , \mathbf{b} in (33). If l_{\min} is not provided, set it to zero. Optional to incorporate further constraints, e.g., (36).
- 4: Define the actual f_{\min} and f_{\max} used in the optimization, which are based on the lowest and highest TRL bands from the longest line that are closest to and include the target frequency range using (6) while setting $\phi = 90^\circ$.
- 5: Define the loss function, e.g., any of (32), (34), or (35).
- 6: Solve for optimal l_2, \dots, l_{N-1} via a global optimization procedure, e.g., using DE method [25].
- 7: **return** Optimized line lengths \mathbf{l}_{opt}

B. Simplified Procedure Using Sparse Rulers

A sparse ruler is a set of marks (numbers) such that every integer distance up to the maximum can be measured as the difference between two marks in the set [27]. For example, the set $\{0, 1, 4, 6\}$ is a sparse ruler because all integer values from 0 to 6 can be obtained as differences between pairs of marks: $\{0, 1, 2, 3, 4, 5, 6\}$. This concept is illustrated in Fig. 9, where a ruler with a subset of marks allows reconstruction of all intermediate positions by taking pairwise differences.

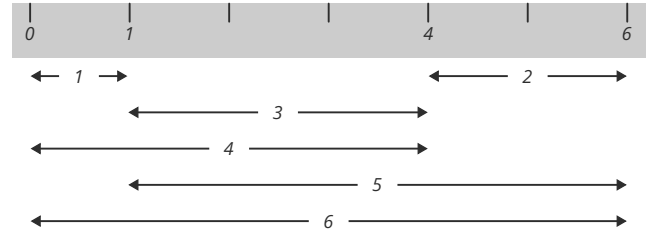


Fig. 9. Illustration of a sparse ruler using the set $\{0, 1, 4, 6\}$, showing how all integer distances from 0 to 6 can be measured using only these four marks.

Sparse rulers are widely used in various applications, such as sensor array design and multi-input, multi-output (MIMO) systems [28], [29]. Their relevance to multiline TRL calibration stems from the fact that the multiline TRL calibration fundamentally depends on the differences between line lengths. As expressed in (16), the eigenvalue λ is composed of the sum over all line pair differences. In the lossless case, this sum is

equivalent to a Fourier series in terms of the line differences, which can be expressed as:

$$\begin{aligned} \lambda \stackrel{\gamma=j\beta}{=} \sum_{\substack{i=1 \\ i < j \leq N}}^{N-1} (e^{j\beta l_{ij}} - e^{-j\beta l_{ij}})^2 &= -4 \sum_{\substack{i=1 \\ i < j \leq N}}^{N-1} \sin^2 \beta l_{ij} \\ &= 2 \sum_{\substack{i=1 \\ i < j \leq N}}^{N-1} (\cos 2\beta l_{ij} - 1) \end{aligned} \quad (37)$$

While (37) is a sum of cosines and a constant term, it becomes a true Fourier series when the line pair differences are integer multiples of a fundamental length. This occurs when $l_{ij} = k_{ij}l_0$, or, in other words, when the lengths are harmonically related. In this case, the eigenvalue simplifies to:

$$\lambda = 2 \sum_{\substack{i=1 \\ i < j \leq N}}^{N-1} (\cos 2\beta l_0 k_{ij} - 1), \quad k_{ij} = k_i - k_j \in \mathbb{N}^+ \quad (38)$$

If the set of k_{ij} covers all integers up to a maximum without gaps, then (38) forms a complete Fourier series. This is the key connection between sparse rulers and multiline TRL calibration: when the line lengths are chosen according to a sparse ruler, all required differences are covered. The line lengths can then be expressed as:

$$l_{\text{ruler}} = \text{Sparse Ruler Set} \times l_0 \quad (39)$$

where l_0 is the smallest step size, i.e., the minimum length difference.

The significance of this Fourier series structure is that the sum of harmonically related sinusoids approaches a square wave as more terms are added. Consequently, the eigenvalue response becomes broader and flatter with an increasing number of line pairs. For example, consider the sets $\{0, 1\}$, $\{0, 1, 3\}$, and $\{0, 1, 4, 6\}$ with $l_0 = 1 \text{ cm}$ and $\epsilon_{r,\text{eff}} = 2.6 - 0j$. As shown in Fig. 10, increasing the number of terms widens the eigenvalue's bandwidth and makes the response more square-like. In Fig. 10, λ is normalized to its maximum value for visualization purposes.

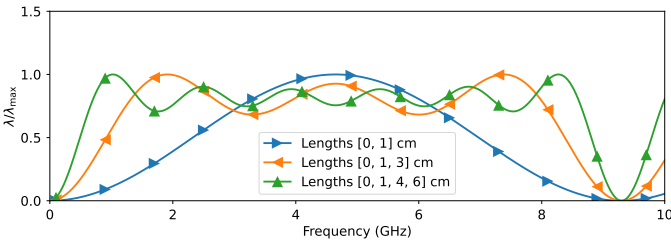


Fig. 10. Comparison of the multiline TRL eigenvalue responses showing how bandwidth increases as larger sparse ruler sets are used ($\{0, 1\}$, $\{0, 1, 3\}$, and $\{0, 1, 4, 6\}$).

In the example shown in Fig. 10, the sparse ruler sets are known as “perfect rulers,” meaning their pairwise differences cover all integers up to the maximum value without redundancy. Only a few perfect rulers exist, such as $\{0, 1\}$, $\{0, 1, 3\}$, and $\{0, 1, 4, 6\}$ [30]. Other types include Wichmann

rulers [31], which cover all differences but with redundancy, and Golomb rulers, which guarantee unique pairwise differences [32], [33]. When Golomb rulers cover all possible differences, they are by definition perfect rulers.

For multiline TRL calibration, there is no strict requirement that the eigenvalue cover all possible differences. In practice, Golomb rulers are often preferred because they avoid redundancy, resulting in a broader bandwidth for a given number of lines compared to Wichmann rulers. Fig. 11 compares the effective phase responses for six lines chosen according to Wichmann and Golomb rulers, with $l_0 = 1 \text{ cm}$ and $\epsilon_{r,\text{eff}} = 2.6 - 0j$. The Golomb set achieves a broader bandwidth by including a longer line, while both sets provide similar effective phase coverage.

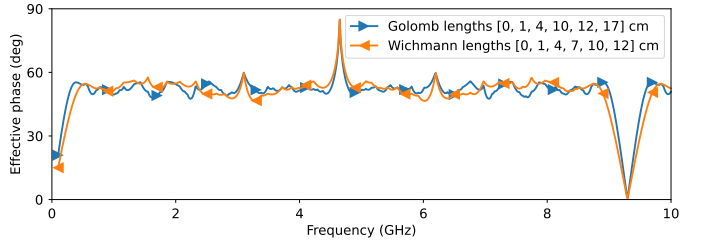


Fig. 11. Comparison of multiline TRL effective phase responses using six lines configurations based on Wichmann and Golomb sparse rulers.

Because sparse rulers generate harmonically related line pairs, the frequency response of the multiline TRL eigenvalue exhibits cyclic banded behavior similar to classical TRL calibration. The minimum and maximum frequencies for each band can be computed using the classical TRL equations from (6). The lower frequency edge is determined by the longest line, while the upper frequency edge is determined by the smallest length difference, l_0 .

Golomb rulers have proven more suitable for multiline TRL calibration in practice because they provide wider bandwidth for a given number of lines, as demonstrated with successful practical multiline TRL kits operating up to 150 GHz [34]–[37]. While the sparse ruler approach offers convenience and simplicity—requiring only the application of TRL equations to determine the frequency range—it lacks an explicit optimality metric, unlike the optimization-based approach discussed in Subsection III-A. This limitation makes it difficult to incorporate loss or frequency-dependent permittivity into the sparse ruler method. Nevertheless, sparse rulers generally perform well in practical applications, even with moderate parameter variations.

The procedure for computing multiline TRL line lengths using sparse rulers is summarized in Algorithm 2.

C. Determining the Recommended Number of Lines

In the lossless case, the general rule is that the longest line determines the lowest frequency, while the shortest line difference sets the highest frequency limit. These limits can be calculated using the classical TRL equations from (6). The purpose of having multiple lines is to fill the gap between the longest and shortest length differences and ensure there are no gaps or nulls in the frequency response of the eigenvalue.

Algorithm 2 Computing line lengths for multiline TRL calibration based on sparse rulers.

Require: Frequency bounds f_{\min} , f_{\max} , average real part of the complex relative effective permittivity $\epsilon_{r,\text{eff}}$, and the thru length defined to be zero, i.e., $l_1 = 0$.

- 1: Compute the minimum line length l_0 from f_{\max} and the desired band of operation using (7b).
- 2: If not provided, determine the number of lines using the procedure in Subsection III-C.
- 3: Select a sparse ruler set (e.g., Golomb or Wichmann) based on the number of lines.
- 4: **return** Multiply l_0 by the sparse ruler set to obtain the line lengths.

For the lossless case, it is possible to develop a procedure to determine the recommended number of lines. However, for the lossy case, this is not straightforward. In lossy media, the relationship changes: longer lines experience higher loss and thus exhibit larger effective phase at higher frequencies. This means the required number of lines depends on the loss characteristics of the transmission medium. In extreme cases, a single long lossy line alongside a thru standard could be sufficient if the loss is significant enough to establish an effective phase above the desired phase margin. Alternatively, for lossy lines, one can perform the optimization procedure discussed in Subsection III-A and incrementally increase the number of lines until the desired effective phase response for the eigenvalue is achieved.

While there is no straightforward way to determine the number of lines for the lossy case beyond the approaches mentioned above, for the lossless case, we can establish a recommended number of lines that ensures sufficient distribution to allow a flat effective phase across the desired frequency range.

Recall that the purpose of using multiple lines is to spread the phase response of each line pair across frequency, creating an effectively constant phase. Without sufficient line lengths between the thru and the longest lines, the nulls of the longest line become the limiting factor of the calibration kit. Therefore, we need enough line pairs to compensate for these nulls across the desired frequency range. For illustration, Fig. 12 shows the eigengap curve of a single long line relative to the thru, highlighting the nulls in the desired frequency range.

In general, each unique line pair shorter than the maximum length difference will have its peak (i.e., 90°) at at least one null of the longest line. Hence, counting the number of nulls in the analyzed frequency range indicates how many line pairs we need. To obtain the recommended line lengths, we first compute the maximum number of line pairs required to cover all nulls of the longest line across the solution frequency range, and from that, derive the appropriate number of lines based on the number of pairs.

To compute the number of nulls in the longest line (i.e., the number of bands), we can use the classical TRL equation for all bands from DC to the solution's maximum frequency. This gives us the maximum number of unique pairs needed to

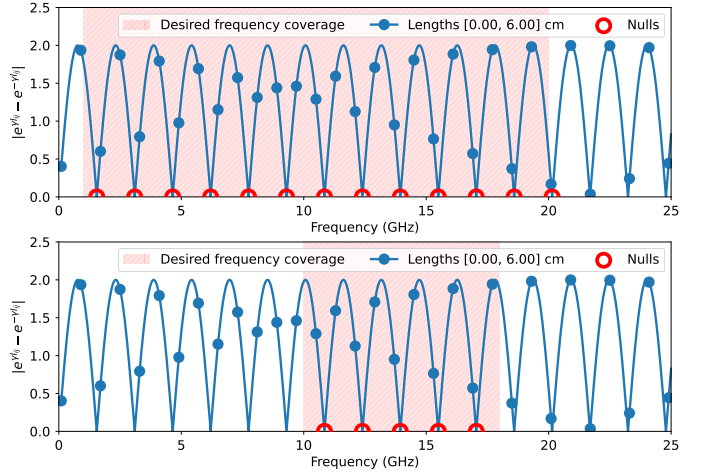


Fig. 12. Illustration of eigenvalue nulls for the longest line within the desired frequency range. The upper plot demonstrates full coverage from DC to f_{\max} , while the lower plot shows a limited bandwidth case between f_{\min} and f_{\max} . In this example, $l_{\max} = 6$ cm and $\epsilon_{r,\text{eff}} = 2.6 - 0j$.

cover all frequencies from DC to f_{\max} :

$$M_{\max} = \left\lceil \frac{2l_{\max}f_{\max}\sqrt{\epsilon'_{r,\text{eff}}}}{c_0} - 1 + \frac{\varphi}{180} \right\rceil + 1 \quad (40)$$

Typically, our lowest desired frequency is above DC, so the actual number of nulls in the eigenvalue of the longest line that are relevant is a function of the bandwidth. We can calculate this by reusing (40) and replacing f_{\max} with the frequency difference, i.e., the bandwidth:

$$M_{\min} = \left\lceil \frac{2l_{\max}(f_{\max} - f_{\min})\sqrt{\epsilon'_{r,\text{eff}}}}{c_0} - 1 + \frac{\varphi}{180} \right\rceil + 1 \quad (41)$$

Note that in both (40) and (41) we round up to the nearest integer to accommodate the phase margin condition, as we want to be one pair above the phase margin limit.

Either (40) or (41) can be used to determine the number of pairs, depending on the desired frequency range and number of lines. When using sparse rulers to generate line lengths, we might not be able to use M_{\min} directly, as it may not satisfy the requirement of a cyclic band structure with harmonically related line lengths. Therefore, we may need to increase M_{\min} until we obtain the closest value that meets the band requirement, which is equivalent to searching for the closest integer that equally divides f_{\max} , since harmonically related lengths must deliver equal bandwidths. Thus, the proper number of line pairs is given by:

$$M = \min\{m \in \{M_{\min}, \dots, M_{\max}\}\}, \quad (42)$$

s.t. $M_{\max} \bmod m = 0$

Finally, the recommended number of lines is computed by inverting the number of pairs equation $M = N(N - 1)/2$, which gives:

$$N = \left\lceil \frac{1 + \sqrt{1 + 8M}}{2} \right\rceil \quad (43)$$

In (43), we choose to round to the nearest integer, because in all of (40)–(42), we are always overestimating the number of pairs. The number of lines determined here remains an approximation; using one more or one less based on rounding is also valid. Determining the truly optimal number of lines ultimately depends on the chosen optimality metric. For example, if the flatness of the eigenvalue is not critical and some dips are acceptable as long as they remain above the specified phase margin, then fewer lines may suffice.

To illustrate this, Fig. 13 shows the equivalent phase for different sets of lines, computed using the number of pairs from (40) and (42), and applying both the optimization and sparse ruler approaches to determine the lengths. In both plots in Fig. 13, the longest line is fixed, and the number of lines is calculated based on the required number of pairs for the coverage bandwidth. In the first plot, (40) is used to calculate full-bandwidth coverage from DC, whereas in the second plot, (42) is used for the limited-bandwidth example.

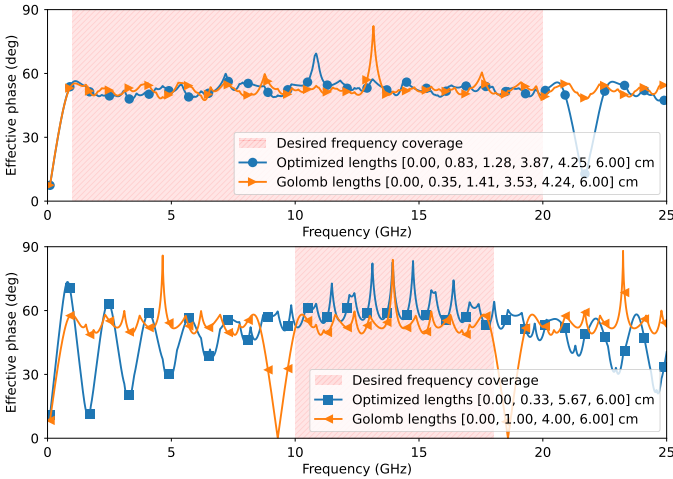


Fig. 13. Effective phase responses for different line sets based on the example in Fig. 12. The upper plot demonstrates full frequency coverage from DC to f_{\max} , while the lower plot shows a limited bandwidth case operating between f_{\min} and f_{\max} . For both cases, $l_{\max} = 6$ cm and $\epsilon_{r,\text{eff}} = 2.6 - 0j$.

IV. NUMERICAL SENSITIVITY ANALYSIS

This section analyzes the line lengths of a multiline TRL calibration kit from a commercial impedance standard substrate (ISS) and compares their sensitivity with those obtained using the procedures proposed in this article, namely the optimization and sparse ruler methods. The ISS under consideration uses CPW lines with the following lengths: $\{0, 0.25, 0.7, 1.6, 3.3, 5.05\}$ mm [38], [39].

The Monte Carlo (MC) analysis uses synthetic data generated by a CPW model [40]–[42], in which all cross-section parameters, including line length, are varied across the different lines. Additive white noise is also included, and the MC analysis was run for 5000 trials. The considered cross-section parameters are shown in Fig. 14.

The uncertainties for the cross-section parameters used in this analysis are listed in Table I, which were taken from [20]. The line length uncertainty is $20 \mu\text{m}$, and additive white noise

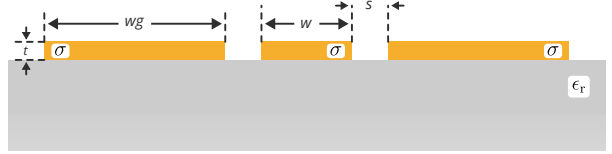


Fig. 14. Geometric cross-section parameters of the CPW structure used in the Monte Carlo analysis. The model uses a lossless Alumina substrate with infinite extent, assuming absorbing boundary conditions.

TABLE I
CROSS-SECTION DIMENSIONS AND MATERIAL PROPERTIES OF THE
CONSIDERED CPW STRUCTURE AND THEIR STANDARD UNCERTAINTIES.

Signal width (μm)	Ground width (μm)	Conductor spacing (μm)	Conductor thickness (μm)	Relative permittivity (1)	Conductor conductivity (S/m)
49.1	273.3	25.5	4.9	9.9	4.11×10^7
± 2.55	± 2.55	± 2.55	± 0.49	± 0.2	$\pm 0.41 \times 10^7$

with a standard deviation of 0.1 is added to the simulated measurements.

Because line lengths in multiline TRL calibration are only relevant through the eigenvalue formulation, we consider only the normalized error terms obtained via eigendecomposition. These normalized error terms are derived from the original error box model in (1) as follows:

$$\tilde{\mathbf{A}} = \begin{bmatrix} 1 & a_{12} \\ a_{21}/a_{11} & 1 \end{bmatrix}; \quad \tilde{\mathbf{B}} = \begin{bmatrix} 1 & b_{12}/b_{11} \\ b_{21} & 1 \end{bmatrix} \quad (44)$$

For the values of the error box model, we assumed ideal thru networks, i.e., $\mathbf{A} = \mathbf{B} = \mathbf{I}$ in (1). This ensures both normalized error boxes $\tilde{\mathbf{A}}$ and $\tilde{\mathbf{B}}$ are equal to identity matrix and are frequency independent. This approach simplifies comparisons across the covered frequency range by eliminating noise shaping by the network response.

We compare the commercial ISS line lengths to an optimized set based on the objective function in (34), as well as to lengths derived from the Golomb sparse ruler. To ensure a fair comparison, we constrain our solutions to match the commercial ISS: the same number of lines, the same maximum length, and quantization in steps of $50 \mu\text{m}$ (i.e., all lengths are some integer multiple of $50 \mu\text{m}$). The results, summarized by the mean absolute error (MAE) over the MC trials and shown in Fig. 15, reveal two frequency regions with apparent differences: 35–50 GHz and 70–90 GHz. Although the commercial ISS line lengths exhibit higher uncertainty in these regions, their performance is otherwise comparable to both the optimized and Golomb sets. There are regions where the commercial ISS line lengths perform better, such as around 60 GHz, but the differences at 35–50 GHz and 70–90 GHz are the most pronounced.

This experiment demonstrates that the optimized line lengths produce a more uniform distribution of error across frequency. This is due to the loss function, which minimizes both the flatness of the eigenvalue and the worst-case value. The behavior also correlates with the inverse eigenvalue of the multiline TRL calibration, which is proportional to the sensitivity of the eigenvectors, as discussed in Section III-A

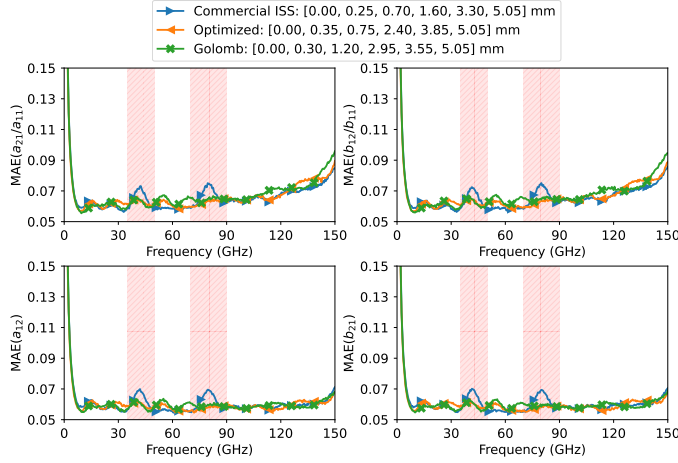


Fig. 15. Monte Carlo analysis results showing the mean absolute error (MAE) of the normalized error terms across frequency for commercial ISS, optimized, and Golomb sparse ruler line length sets.

and (30). Fig. 16 illustrates this, showing that the frequency ranges with higher mean absolute error in the MC analysis also correspond to higher inverse eigenvalue for the commercial ISS line lengths, compared to the optimized and Golomb sets.

Furthermore, the analysis shows that using Golomb sparse ruler lengths achieves performance comparable to the optimized lengths, while requiring significantly less computation time. The optimization process used the differential evolution (DE) method [25], [43], which took about 10 minutes to complete with 2000 iterations on a modern multicore processor. In contrast, the Golomb sparse ruler lengths were obtained instantly using a precomputed table [44].

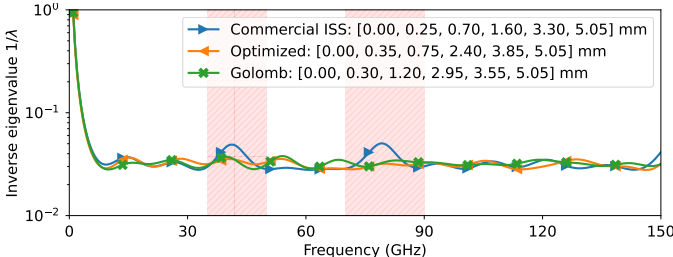


Fig. 16. Comparison of inverse eigenvalues across frequency for commercial ISS, optimized, and Golomb sparse ruler line length sets.

V. DESIGN EXAMPLES

A. Exploiting Dispersive Conductors in Transmission Lines

Many planar transmission line implementations use conductors with small cross-sectional dimensions, such as thin-film microstrip lines (TFMSL) [45]. Small conductors increase internal inductance, which raises the relative effective permittivity at low frequencies. This effect is further exacerbated by multilayer metallization, for example, electroless nickel immersion gold (ENIG) plating that incorporates ferromagnetic metals such as nickel [46]. Additionally, frequency dependency in the relative effective permittivity also arises from geometry; for instance, a microstrip is typically more dispersive than a CPW line.

In this example, we use the TFMSL structure based on the model from [45] with its cross-section shown in Fig. 17 and parameter values provided in the caption.

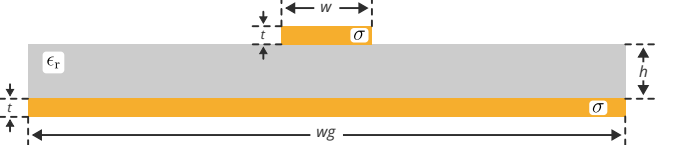


Fig. 17. Thin-film microstrip line cross-section parameters from [45]: substrate permittivity $\epsilon_r = 2.7(1 - j0.015)$, conductor conductivity $\sigma = 25 \text{ MS/m}$, metal thickness $t = 0.8 \mu\text{m}$, strip width $w = 8 \mu\text{m}$, substrate height $h = 1.7 \mu\text{m}$, and ground plane width $wg = 88 \mu\text{m}$.

Due to the small dimensions, the relative effective permittivity of this structure is strongly frequency-dependent: it is high at low frequencies and decreases toward the substrate permittivity at higher frequencies. This behavior is shown in Fig. 18. Because both the substrate and conductors are lossy, the attenuation per unit length also increases noticeably with frequency.

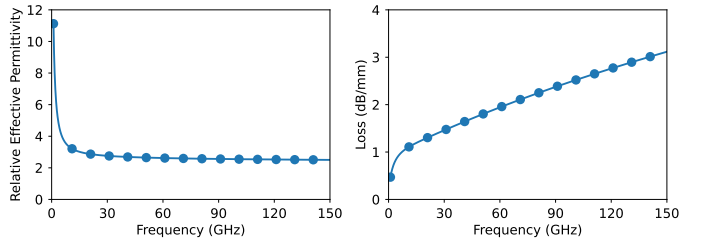


Fig. 18. Frequency response of the thin-film microstrip line in Fig. 17, showing relative effective permittivity and attenuation per unit length.

To exploit this dispersion, we compute optimized lengths for two cases. In the first, we assume lossless, frequency-independent relative effective permittivity. In the second, we supply the frequency-dependent relative effective permittivity directly to the optimizer.

As the internal inductance raises the effective permittivity at low frequencies, shorter lines are sufficient under this condition compared to those predicted using only a constant relative effective permittivity. For our constant permittivity case, we used the median value of the frequency-dependent response to avoid the low-frequency outliers caused by internal inductance. With loss included, the optimal length distribution changes accordingly, typically reducing the required number of lines.

Fig. 19 presents the effective phase of the computed lines. As expected, using the frequency-dependent model yields substantially shorter lengths and fewer lines while covering the same frequency range. Both runs used the same settings with the loss function in (34) and a $10 \mu\text{m}$ length standard deviation and quantized lengths in steps of $50 \mu\text{m}$.

B. On-Wafer Multiline TRL Lengths for THz Frequencies

Capabilities for measurements at sub-THz and THz frequencies are getting increasingly important in industry and research [47]–[49]. Careful design of a multiline TRL calibration kit

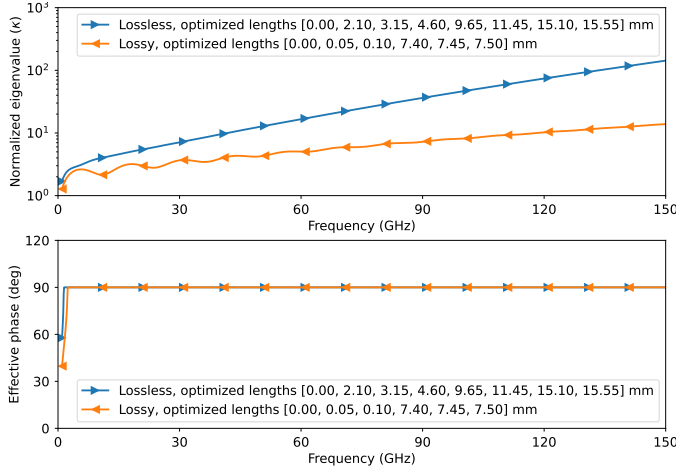


Fig. 19. Comparison of effective phase for the thin-film microstrip multiline TRL lines optimized under two scenarios: constant lossless relative effective permittivity versus frequency-dependent dispersive, lossy relative effective permittivity.

is therefore essential to span such wide bandwidths. In this example, we compute lengths for a multiline TRL calibration kit implemented as CPW on an Alumina substrate. We focus only on length design; for cross-sectional geometry choices, see, for example, [50].

In the absence of specific geometry, we assume a typical average relative effective permittivity for CPW on Alumina, $\epsilon_{r,\text{eff}} \approx 5.2$, and neglect loss. In practice, materials are dispersive, as illustrated in Subsection V-A.

The frequency range is 2 GHz to 1.1 THz with a 30° low-frequency phase margin. The computed lines and their effective phase are shown in Fig. 20. Two methods are used: (i) the optimization method from Subsection III-A with the loss function (34) and a 10 μm length standard deviation. The maximum line length is set by the 2 GHz requirement and the 30° phase margin; the number of lines then follows from that maximum length and the 1.1 THz upper limit. (ii) a Golomb sparse ruler approach subject to the same constraints.

Fig. 20 shows that 14 lines suffice to cover 2 GHz to 1.1 THz with a nearly flat effective phase. Because this analysis assumes a generic lossless CPW on an Alumina substrate, a specific geometry that includes conductor loss and dispersion will require fewer lines, since higher effective permittivity at low frequencies and higher loss at high frequencies both reduce the required maximum length and the number of lines.

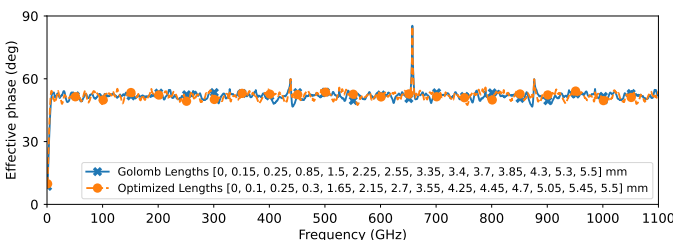


Fig. 20. Effective phase up to 1.1 THz for optimized generic CPW multiline TRL calibration lengths on lossless Alumina substrate.

C. Waveguide Multiline Kit Using Longer Lines

Defining a TRL calibration kit for a waveguide is straightforward when using the traditional quarter-wavelength line, which spans the waveguide bandwidth, and the quarter-wavelength phase of the line is set in the middle of the band. However, as the frequency increases, the quarter-wavelength line becomes very short and increasingly difficult to manufacture because feature sizes approach typical fabrication tolerances, especially with additive processes such as 3D-printed waveguides [51].

A multiline TRL approach enables the use of longer lines. For example, “3/4-wave” or “5/4-wave” TRL kits exploit the cyclic nature of TRL: two longer lines are combined to realize a multiline TRL in waveguide [6]–[8].

Here, we generalize the design of a waveguide multiline TRL calibration kit by imposing a maximum manufacturable line length and then computing the number of lines and their lengths automatically, using the proposed optimization procedure under the imposed constraints.

We consider the WM-864 waveguide, operating from 220 GHz to 300 GHz, with width 864 μm and height 432 μm [52]. The waveguide model used to compute the relative effective permittivity follows [53], [54]. To obtain lengths robust to fabrication tolerances, we use the loss function (34) with a 10 μm length standard deviation to model sensitivity to length variation. The maximum line length is limited to 5 mm, which sets the number of lines; changing this limit adjusts the count. The optimized results in Fig. 21 exhibit a flatter effective phase and are compared with those of a conventional quarter-wavelength TRL kit. The optimized multiline TRL kit requires four lines, whereas the quarter-wavelength kit requires two. The longer lines in the multiline kit are easier to fabricate and less sensitive to length variation.

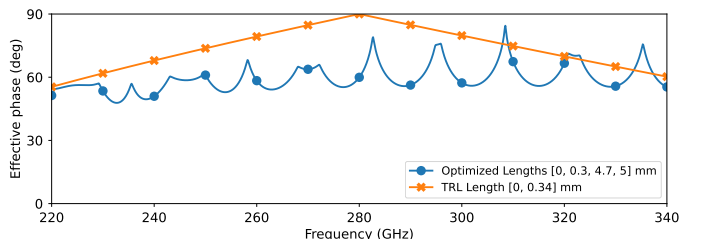


Fig. 21. Comparison of effective phase versus frequency for the optimized multiline TRL calibration kit and a conventional quarter-wavelength TRL kit for WM-864 waveguide.

VI. CONCLUSION

We present a rigorous analysis and design procedure for selecting optimal lengths for line standards in multiline TRL calibration. First, we develop an effective phase metric that enables fair comparison across length sets, even when they differ in the number of lines. We then introduce two methods for choosing the lengths: a brute-force optimization and a sparse-ruler approach. The optimization method is general and applies to any transmission line type, including dispersive and lossy media, while the sparse-ruler approach is fast and leverages precomputed ruler marks, as Golomb rulers.

We also discussed the recommended number of lines by focusing on bandwidth coverage rather than maximum frequency, which can reduce the required line count when only limited bandwidth is needed. Next, we performed a sensitivity analysis via Monte Carlo simulation, comparing a commercial ISS length set based on a CPW structure with optimized lengths constrained to the same maximum length and line count. The optimized lengths yield a flatter uncertainty response. Finally, we provide design examples for computing line lengths, including cases with dispersive materials, THz frequencies, and waveguide-based multiline TRL.

APPENDIX A SCALING THE WEIGHTING MATRIX IN MULTILINE TRL CALIBRATION

The weighting matrix for multiline TRL calibration, as described in [4], [20] and defined in (14), formulates the eigenvalue problem based on all line measurements. This matrix effectively performs self-weighting of the line pairs. The weighting mechanism can be modified by scaling the matrix entries to achieve specific calibration objectives. Common reasons for such scaling include distributing the weight of repeated lines according to their occurrence, enhancing selectivity by increasing the weighting order beyond the default L1-norm, and implementing customized weighting schemes.

To incorporate scaling, we introduce a nonzero symmetric matrix \mathbf{S} and apply the Hadamard product [22]:

$$\mathbf{W}_S = \mathbf{S} \odot \mathbf{W} \quad (45)$$

where \odot denotes the Hadamard (element-wise) product. In the special case where $\mathbf{S} = \mathbf{1}\mathbf{1}^T$, with $\mathbf{1} = [1 \ 1 \ \dots]^T$, the scaling has no effect and $\mathbf{W}_S = \mathbf{W}$.

The eigenvalue problem of multiline TRL calibration in (14) is updated by simply substituting \mathbf{W}_S in place of \mathbf{W} . The eigenvalue λ and normalized eigenvalue κ are also updated to take the following form:

$$\lambda_S = \frac{1}{2} \text{vec}(\mathbf{W}_S)^H \text{vec}(\mathbf{W}), \quad \kappa_S = \frac{2\lambda_S}{\|\text{vec}(\mathbf{W}_S)\|_1} \quad (46)$$

One application for scaling the weighting matrix is to weight repeated lines by their occurrence. For example, consider four lines with the third line repeated, i.e., $[l_1, l_2, l_3, l_3]$. A suitable scaling matrix is defined as follows:

$$\mathbf{S} = \mathbf{q}\mathbf{q}^T = \begin{bmatrix} \cancel{1} & 1 & 1/2 & 1/2 \\ 1 & \cancel{1} & 1/2 & 1/2 \\ 1/2 & 1/2 & \cancel{1/4} & \cancel{1/4} \\ 1/2 & 1/2 & \cancel{1/4} & \cancel{1/4} \end{bmatrix} \quad (47)$$

where $\mathbf{q} = [1 \ 1 \ 1/2 \ 1/2]^T$. The crossed entries are “don’t-care” values and may be set to zero, since the corresponding entries of \mathbf{W} are by definition zero for line pairs of equal length. The vector \mathbf{q} contains the weights of the lines based on their occurrence. If all lines are unique, then $\mathbf{q} = \mathbf{1}$ and the scaling has no effect.

As an example, consider the length sets $[0, 1, 4, 6]$ cm and $[0, 1, 4, 6, 6, 6]$ cm. The second set includes the 6 cm line three times, hence $\mathbf{q} = [1 \ 1 \ 1 \ 1/3 \ 1/3 \ 1/3]^T$. Fig. 22

shows the effective phase for both sets; the second set is plotted twice, with and without scaling. The scaled version matches the effective phase of the four-line set without redundancy.

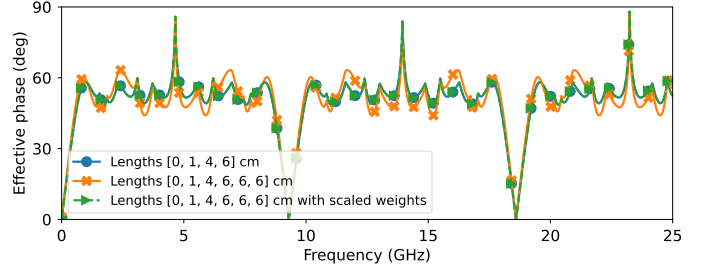


Fig. 22. Effective phase comparison in multiline TRL calibration using two different line sets: a four-line set $\{0, 1, 4, 6\}$ cm and a six-line set $\{0, 1, 4, 6, 6, 6\}$ cm with the 6 cm line repeated three times. The plot compares standard and scaled weighting approaches for the six-line set. All curves assume a relative effective permittivity of $\epsilon_{r,\text{eff}} = 2.6$.

Another application of scaling the weighting matrix is to make the weighting more selective. The standard weighting is based on the L1-norm, where each line pair is weighted by its eigengap. This can be modified by:

$$\mathbf{W}_m = |\mathbf{W}|^{\odot(m-1)} \odot \mathbf{W} \quad (48)$$

where $|\cdot|$ and $(\cdot)^{\odot(m-1)}$ denote element-wise absolute value and element-wise exponentiation to the power $m-1$, respectively. The default is $m = 1$. Higher values of m establish the Lm -norm for line pair weighting and progressively bias the effective phase toward line pairs with larger phase differences. In the extreme case as $m \rightarrow \infty$, we have $L\infty$ -norm weighting, where at each frequency only the line pair with maximum phase difference is selected. Increasing the order too much reduces the averaging effect and biases the result toward line pairs with the largest phase difference. Fig. 23 shows the effective phase for several weighting orders. It should be kept in mind that taking high exponentiation in software leads to numerical instability. Hence, only the cases $m = 1$ and $m = 2$ are usually stable in software implementation.

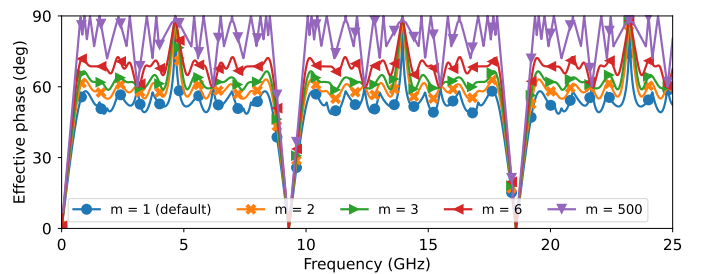


Fig. 23. Effective phase comparison for the line set $\{0, 1, 4, 6\}$ cm calculated with relative effective permittivity $\epsilon_{r,\text{eff}} = 2.6$, showing the impact of different Lm -norm weighting orders.

APPENDIX B

COMPUTING THE JACOBIAN OF THE MULTILINE TRL
EIGENVALUE WITH RESPECT TO LINE LENGTHS

The Jacobian of λ with respect to the line lengths is defined as

$$\mathbf{J}_\lambda(\mathbf{l}, f) = \begin{bmatrix} \frac{\partial \lambda(\mathbf{l}, f)}{\partial l_1} & \frac{\partial \lambda(\mathbf{l}, f)}{\partial l_2} & \dots & \frac{\partial \lambda(\mathbf{l}, f)}{\partial l_N} \end{bmatrix}. \quad (49)$$

To compute this Jacobian, we need to determine each partial derivative with respect to the i th length. These derivatives can be obtained directly from (16) in summation form:

$$\frac{\partial \lambda(\mathbf{l}, f)}{\partial l_i} = \sum_{j \neq i}^N \frac{\partial}{\partial l_i} |e^{\gamma l_{ij}} - e^{-\gamma l_{ij}}|^2, \quad (50)$$

where $l_{ij} = l_i - l_j$.

For notational convenience, we define $w_{ij} = e^{\gamma l_{ij}} - e^{-\gamma l_{ij}}$. Using principles from complex-valued calculus [55], the partial derivative in (50) can be expressed as

$$\frac{\partial \lambda(\mathbf{l}, f)}{\partial l_i} = 2 \sum_{j \neq i}^N \operatorname{Re} \left(w_{ij}^* \frac{\partial w_{ij}}{\partial l_i} \right), \quad (51)$$

where $\operatorname{Re}(\cdot)$ denotes the real part and w_{ij}^* is the complex conjugate of w_{ij} . Computing the derivative of w_{ij} yields

$$\frac{\partial \lambda(\mathbf{l}, f)}{\partial l_i} = 2 \sum_{j \neq i}^N \operatorname{Re} \left(\gamma w_{ij}^* (e^{\gamma l_{ij}} + e^{-\gamma l_{ij}}) \right). \quad (52)$$

REFERENCES

- [1] G. Engen and C. Hoer, "Thru-reflect-line: An improved technique for calibrating the dual six-port automatic network analyzer," *IEEE Transactions on Microwave Theory and Techniques*, vol. 27, no. 12, pp. 987–993, 1979, doi: [10.1109/TMTT.1979.1129778](https://doi.org/10.1109/TMTT.1979.1129778).
- [2] U. Stumper, "Uncertainty of vna s-parameter measurement due to nonideal trl calibration items," *IEEE Transactions on Instrumentation and Measurement*, vol. 54, no. 2, pp. 676–679, 2005.
- [3] R. Marks, "A multiline method of network analyzer calibration," *IEEE Transactions on Microwave Theory and Techniques*, vol. 39, no. 7, pp. 1205–1215, 1991, doi: [10.1109/22.85388](https://doi.org/10.1109/22.85388).
- [4] Z. Hatab, M. Gadringer, and W. Bösch, "Improving the reliability of the multiline trl calibration algorithm," in *2022 98th ARFTG Microwave Measurement Conference (ARFTG)*. IEEE, Jan. 2022, doi: [10.1109/ARFTG52954.2022.9844064](https://doi.org/10.1109/ARFTG52954.2022.9844064). pp. 1–5.
- [5] Microwaves101, "TRL-calibration — microwaves101.com," <https://www.microwaves101.com/encyclopedia/trl-calibration>, [Accessed 15-01-2024].
- [6] N. M. Ridler, "Choosing line lengths for calibrating waveguide vector network analysers at millimetre and sub-millimetre wavelengths," NPL Report, March 2009. [Online]. Available: <http://eprintspublications.npl.co.uk/4346/>
- [7] N. M. Ridler, R. G. Clarke, C. Li, and M. J. Salter, "Strategies for traceable submillimeter-wave vector network analyzer," *IEEE Transactions on Terahertz Science and Technology*, vol. 9, no. 4, pp. 392–398, Jul. 2019, doi: [10.1109/TTHZ.2019.2911870](https://doi.org/10.1109/TTHZ.2019.2911870).
- [8] N. M. Ridler, S. Johny, M. J. Salter, X. Shang, W. Sun, and A. Wilson, "Establishing waveguide lines as primary standards for scattering parameter measurements at submillimetre wavelengths," *Metrologia*, vol. 58, no. 1, p. 015015, jan 2021, doi: [10.1088/1681-7575/abd371](https://doi.org/10.1088/1681-7575/abd371).
- [9] H.-J. Eul and B. Schiek, "Thru-match-reflect: One result of a rigorous theory for de-embedding and network analyzer calibration," in *1988 18th European Microwave Conference*. IEEE, Sep. 1988, doi: [10.1109/euma.1988.333924](https://doi.org/10.1109/euma.1988.333924). pp. 909–914.
- [10] D. DeGroot, J. Jargon, and R. Marks, "Multiline trl revealed," in *60th ARFTG Conference Digest, Fall 2002*, ser. ARFTG-02. IEEE, 2002, doi: [10.1109/ARFTG.2002.1218696](https://doi.org/10.1109/ARFTG.2002.1218696). pp. 131–155.
- [11] D. Williams, C. Wang, and U. Arz, "An optimal multiline trl calibration algorithm," in *IEEE MTT-S International Microwave Symposium Digest, 2003*, ser. MWSYM-03, vol. 3. IEEE, 2003, doi: [10.1109/MWSYM.2003.1210494](https://doi.org/10.1109/MWSYM.2003.1210494). pp. 1819–1822 vol.3.
- [12] C. Hoer, "Choosing line lengths for calibrating network analyzers," *IEEE Transactions on Microwave Theory and Techniques*, vol. 31, no. 1, pp. 76–78, 1983, doi: [10.1109/TMTT.1983.1131433](https://doi.org/10.1109/TMTT.1983.1131433).
- [13] C. A. Hoer, "Some questions and answers concerning air lines as impedance standards," in *29th ARFTG Conference Digest*, vol. 11, 1987, doi: [10.1109/ARFTG.1987.323862](https://doi.org/10.1109/ARFTG.1987.323862). pp. 161–173.
- [14] J. Reynoso-Hernandez, "Reliable method for computing the phase shift of multiline trl calibration technique," *IEEE Microwave and Wireless Components Letters*, vol. 12, no. 10, pp. 395–397, Oct. 2002, doi: [10.1109/lmwc.2002.804572](https://doi.org/10.1109/lmwc.2002.804572).
- [15] S.-H. Shin, M. Stanley, J. Skinner, S. E. de Graaf, and N. M. Ridler, "Broadband coaxial s-parameter measurements for cryogenic quantum technologies," *IEEE Transactions on Microwave Theory and Techniques*, vol. 72, no. 4, pp. 2193–2201, Apr. 2024, doi: [10.1109/tmtt.2023.3322909](https://doi.org/10.1109/tmtt.2023.3322909).
- [16] C. A. Hoer and G. F. Engen, "On-line accuracy assessment for the dual six-port ana: Extension to nonmating connectors," *IEEE Transactions on Instrumentation and Measurement*, vol. IM-36, no. 2, pp. 524–529, 1987, doi: [10.1109/TIM.1987.6312732](https://doi.org/10.1109/TIM.1987.6312732).
- [17] R. Marks and D. Williams, "A general waveguide circuit theory," *Journal of Research (NIST JRES), National Institute of Standards and Technology, Gaithersburg, MD*, no. 97, 1992, doi: [10.6028/jres.097.024](https://doi.org/10.6028/jres.097.024).
- [18] M. Steer, *Microwave and RF Design: Transmission Lines, Volume 2*. NC State University, Jul. 2019. ISBN 9781469656939
- [19] J. Brewer, "Kronecker products and matrix calculus in system theory," *IEEE Transactions on Circuits and Systems*, vol. 25, no. 9, pp. 772–781, Sep. 1978, doi: [10.1109/tcs.1978.1084534](https://doi.org/10.1109/tcs.1978.1084534).
- [20] Z. Hatab, M. E. Gadringer, and W. Bösch, "Propagation of linear uncertainties through multiline thru-reflect-line calibration," *IEEE Transactions on Instrumentation and Measurement*, vol. 72, pp. 1–9, 2023, doi: [10.1109/TIM.2023.3296123](https://doi.org/10.1109/TIM.2023.3296123).
- [21] J. H. Wilkinson, *The algebraic eigenvalue problem*, reprinted from corr. sheets of the 1. ed. ed., ser. Monographs on numerical analysis. Oxford: Clarendon Press, 1978. ISBN 0198534035
- [22] L. Hogben, Ed., *Handbook of linear algebra*, second edition. ed., ser. Discrete mathematics and its applications. Boca Raton: CRC Press, 2014. ISBN 9781466507296 Includes bibliographical references. Description based on print version record. "A Chapman & Hall book."
- [23] A. Lann and R. Falk, "Tell me the method, i'll give you the mean," *The American Statistician*, vol. 60, no. 4, pp. 322–327, Nov. 2006, doi: [10.1198/000313006x151460](https://doi.org/10.1198/000313006x151460).
- [24] J. R. Magnus, "On differentiating eigenvalues and eigenvectors," *Econometric Theory*, vol. 1, no. 2, pp. 179–191, 1985. [Online]. Available: <http://www.jstor.org/stable/3532409>
- [25] R. Storn and K. Price, "Differential evolution – a simple and efficient heuristic for global optimization over continuous spaces," *Journal of Global Optimization*, vol. 11, no. 4, pp. 341–359, Dec. 1997, doi: [10.1023/a:1008202821328](https://doi.org/10.1023/a:1008202821328).
- [26] J. Lampinen, "A constraint handling approach for the differential evolution algorithm," in *Proceedings of the 2002 Congress on Evolutionary Computation. CEC'02 (Cat. No.02TH8600)*, ser. CEC-02, vol. 2. IEEE, 2002, doi: [10.1109/cec.2002.1004459](https://doi.org/10.1109/cec.2002.1004459). pp. 1468–1473.
- [27] D. Linebarger, I. Sudborough, and I. Tollis, "Difference bases and sparse sensor arrays," *IEEE Transactions on Information Theory*, vol. 39, no. 2, pp. 716–721, Mar. 1993, doi: [10.1109/18.212309](https://doi.org/10.1109/18.212309).
- [28] H. Xiao, B. Zhou, Y. Zhang, and G. Xiao, "On the foundation of sparsity constrained sensing—part ii: Diophantine sampling with arbitrary temporal and spatial sparsity," *IEEE Transactions on Signal Processing*, vol. 71, pp. 1277–1292, 2023, doi: [10.1109/tsp.2023.3248493](https://doi.org/10.1109/tsp.2023.3248493).
- [29] D. Romero, D. D. Ariananda, Z. Tian, and G. Leus, "Compressive covariance sensing: Structure-based compressive sensing beyond sparsity," *IEEE Signal Processing Magazine*, vol. 33, no. 1, pp. 78–93, Jan. 2016, doi: [10.1109/msp.2015.2486805](https://doi.org/10.1109/msp.2015.2486805).
- [30] J. Leech, "On the representation of 1, 2, ..., n by differences," *Journal of the London Mathematical Society*, vol. s1-31, no. 2, pp. 160–169, Apr. 1956, doi: [10.1112/jlms/s1-31.2.160](https://doi.org/10.1112/jlms/s1-31.2.160).
- [31] B. Wichmann, "A note on restricted difference bases," *Journal of the London Mathematical Society*, vol. s1-38, no. 1, pp. 465–466, 1963, doi: [10.1112/jlms/s1-38.1.465](https://doi.org/10.1112/jlms/s1-38.1.465).
- [32] S. Sidon, "Ein satz ueber trigonometrische polynome und seine anwendung in der theorie der fourier-reihen," *Mathematische Annalen*, vol. 106, no. 1, pp. 536–539, Dec. 1932, doi: [10.1007/bf01455900](https://doi.org/10.1007/bf01455900).

[33] C. Meyer and P. A. Papakonstantinou, "On the complexity of constructing golomb rulers," *Discrete Applied Mathematics*, vol. 157, no. 4, pp. 738–748, Feb. 2009, doi: [10.1016/j.dam.2008.07.006](https://doi.org/10.1016/j.dam.2008.07.006).

[34] Z. Hatab, M. E. Gadringer, and W. Bösch, "A thru-free multiline calibration," *IEEE Transactions on Instrumentation and Measurement*, vol. 72, pp. 1–9, 2023, doi: [10.1109/TIM.2023.3308226](https://doi.org/10.1109/TIM.2023.3308226).

[35] Z. Hatab, H. Takahashi, A. B. A. Alterkawi, M. E. Gadringer, and W. Bösch, "A quasi-tem approach for designing microvias for pcb layer transition with minimal return loss," in *2023 53rd European Microwave Conference (EuMC)*, 2023, doi: [10.23919/EuMC58039.2023.10290259](https://doi.org/10.23919/EuMC58039.2023.10290259), pp. 62–65.

[36] A. Arsanjani, A. Abdi, Z. Hatab, A. B. Alothman Alterkawi, M. Ernst Gadringer, and W. Bösch, "Miniaturized ka-band metasurface filter with wide out-of-band rejection up to the 5th harmonic," in *2024 54th European Microwave Conference (EuMC)*, 2024, doi: [10.23919/EuMC61614.2024.10732666](https://doi.org/10.23919/EuMC61614.2024.10732666), pp. 188–191.

[37] A. Arsanjani, Z. Hatab, A. B. A. Alterkawi, M. E. Gadringer, and W. Bösch, "Modified semi-additive manufacturing of pcbs for enabling accurate device measurements at millimeter-wave and sub-terahertz frequencies," in *2024 103rd ARFTG Microwave Measurement Conference (ARFTG)*, 2024, doi: [10.1109/ARFTG61196.2024.10660794](https://doi.org/10.1109/ARFTG61196.2024.10660794), pp. 1–4.

[38] FormFactor Inc., "Impedance standard substrate (iss) 104-783: 75-150 um pitch, up to 145 ghz," 2023, [Accessed 15-01-2024]. [Online]. Available: <https://www.formfactor.com/product/probes/calibration-tools-probes/impedance-standard-substrates/>

[39] MPI Corporation, "Ac2-2 calibration substrate: 100-250 um pitch, up to 110 ghz," 2023, [Accessed 15-01-2024]. [Online]. Available: <https://www.mpi-corporation.com/ast/mpi-rf-probes-accessories/mpi-rf-calibration-substrates/>

[40] G. N. Phung and U. Arz, "On the influence of thru- and line-length-related effects in cpw- based multiline trl calibrations," in *2021 97th ARFTG Microwave Measurement Conference (ARFTG)*, 2021, doi: [10.1109/ARFTG52261.2021.9639909](https://doi.org/10.1109/ARFTG52261.2021.9639909), pp. 1–4.

[41] F. Schnieder, T. Tischler, and W. Heinrich, "Modeling dispersion and radiation characteristics of conductor-backed cpw with finite ground width," *IEEE Transactions on Microwave Theory and Techniques*, vol. 51, no. 1, pp. 137–143, Jan. 2003, doi: [10.1109/tmtt.2002.806926](https://doi.org/10.1109/tmtt.2002.806926).

[42] W. Heinrich, "Quasi-tem description of mmic coplanar lines including conductor-loss effects," *IEEE Transactions on Microwave Theory and Techniques*, vol. 41, no. 1, pp. 45–52, 1993, doi: [10.1109/22.210228](https://doi.org/10.1109/22.210228).

[43] P. Virtanen *et al.*, "SciPy 1.0: Fundamental Algorithms for Scientific Computing in Python," *Nature Methods*, vol. 17, pp. 261–272, 2020, doi: [10.1038/s41592-019-0686-2](https://doi.org/10.1038/s41592-019-0686-2).

[44] distributed.net, "Project ogr - distributed.net," <https://www.distributed.net/ogr>, 2024, accessed: 2025-01-15. [Online]. Available: <https://www.distributed.net/ogr>

[45] F. Schnieder and W. Heinrich, "Model of thin-film microstrip line for circuit design," *IEEE Transactions on Microwave Theory and Techniques*, vol. 49, no. 1, pp. 104–110, 2001, doi: [10.1109/22.899967](https://doi.org/10.1109/22.899967).

[46] B. Schafsteller, M. Schwaemmlein, M. Rosin, G. Ramos, Z. Hatab, M. E. Gadringer, and E. Schlaffer, "Investigating the impact of final finishes on the insertion loss in as received and after aging," *IMAPSsource Proceedings*, vol. 2023, no. Symposium, Feb. 2024, doi: [10.4071/001c.94519](https://doi.org/10.4071/001c.94519).

[47] L. Chen *et al.*, "Terahertz micromachined on-wafer probes: Repeatability and reliability," *IEEE Transactions on Microwave Theory and Techniques*, vol. 60, no. 9, pp. 2894–2902, Sep. 2012, doi: [10.1109/tmtt.2012.2205016](https://doi.org/10.1109/tmtt.2012.2205016).

[48] M. F. Bauwens, N. Aljabbari, A. W. Lichtenberger, N. S. Barker, and R. M. Weikle, "A 1.1 thz micromachined on-wafer probe," in *2014 IEEE MTT-S International Microwave Symposium (IMS2014)*. IEEE, Jun. 2014, doi: [10.1109/mwsym.2014.6848607](https://doi.org/10.1109/mwsym.2014.6848607).

[49] S. Fregonese, M. Deng, M. Cabbia, C. Yadav, M. De Matos, and T. Zimmer, "Thz characterization and modeling of sige hbts: Review (invited)," *IEEE Journal of the Electron Devices Society*, vol. 8, pp. 1363–1372, 2020, doi: [10.1109/jeds.2020.3036135](https://doi.org/10.1109/jeds.2020.3036135).

[50] M. Spirito, U. Arz, G. N. Phung, F. J. Schmückle, W. Heinrich, and R. Lozar, "Guidelines for the design of calibration substrates, including the suppression of parasitic modes for frequencies up to and including 325 ghz : Empir 14ind02," 2019, doi: [10.7795/530.20190424A](https://doi.org/10.7795/530.20190424A).

[51] L. Zhu, S.-H. Shin, R. Payapulli, I. W. Rossuck, N. Klein, N. M. Ridler, and S. Lucyszyn, "3-d printed thz waveguide components," *IEEE Access*, vol. 11, pp. 79 073–79 086, 2023, doi: [10.1109/access.2023.3297271](https://doi.org/10.1109/access.2023.3297271).

[52] "Ieee standard for rectangular metallic waveguides and their interfaces for frequencies of 110 ghz and above—part 1: Frequency bands and waveguide dimensions," *IEEE Std 1785.1-2012*, pp. 1–22, 2013, doi: [10.1109/IEEESTD.2013.6471987](https://doi.org/10.1109/IEEESTD.2013.6471987).

[53] K. Lomakin, G. Gold, and K. Helmreich, "Transmission line model for rectangular waveguides accurately incorporating loss effects," in *2017 IEEE 21st Workshop on Signal and Power Integrity (SPI)*. IEEE, May 2017, doi: [10.1109/sapiw.2017.7944024](https://doi.org/10.1109/sapiw.2017.7944024), pp. 1–4.

[54] ———, "Analytical waveguide model precisely predicting loss and delay including surface roughness," *IEEE Transactions on Microwave Theory and Techniques*, vol. 66, no. 6, pp. 2649–2662, Jun. 2018, doi: [10.1109/tmtt.2018.2827383](https://doi.org/10.1109/tmtt.2018.2827383).

[55] T. Needham and R. Penrose, *Visual Complex Analysis: 25th Anniversary Edition*. Oxford University PressOxford, Feb. 2023. ISBN 9780191964947